Developmental Biology 453 (2019) 141–154

Contents lists available at ScienceDirect

Developmental Biology

journal homepage: www.elsevier.com/locate/developmentalbiology

Targeted deletion of Crb1/Crb2 in the optic vesicle models key features of leber congenital amaurosis 8

Seo-Hee Cho [a,*], Ankur Nahar [a], Ji Hyang Kim [a], Matthew Lee [a], Zbynek Kozmik [b], Seonhee Kim [a]

[a] Shriners Hospitals Pediatric Research Center, Department of Anatomy and Cell Biology, Lewis Katz School of Medicine, Temple University, Philadelphia, PA, 19140, USA
[b] Institute of Molecular Genetics, Academy of Sciences of the Czech Republic, Prague, Czech Republic

ARTICLE INFO

Keywords:
Leber congenital amaurosis 8
Crumbs
Crb1/Crb2
Polarity
And retinal progenitor cells

ABSTRACT

The Crb1 and 2 (Crumbs homolog 1 & 2) genes encode large, single-pass transmembrane proteins essential for the apicobasal polarity and adhesion of epithelial cells. Crb1 mutations cause degenerative retinal diseases in humans, including Leber congenital amaurosis type 8 (LCA8) and retinitis pigmentosa type 12 (RP12). In LCA8, impaired photoreceptor development and/or survival is thought to cause blindness during early infancy, whereas, in RP12, progressive photoreceptor degeneration damages peripheral vision later in life. There are multiple animal models of RP12 pathology, but no experimental model of LCA8 recapitulates the full spectrum of its pathological features. To generate a mouse model of LCA8 and identify the functions of Crb1/2 in developing ocular tissues, we used an mRx-Cre driver to generate allelic combinations that enabled conditional gene ablation from the optic vesicle stage. In this series only Crb1/2 double knockout (dKO) mice exhibited characteristics of human LCA8 disease: locally thickened retina with spots devoid of cells, aberrant positioning of retinal cells, severely disrupted lamination, and depigmented retinal-pigmented epithelium. Retinal defects antedated E12.5, which is far earlier than the stage at which photoreceptor cells mainly differentiate. Most remarkably, Crb1/Crb2 dKO showed a severely attenuated electroretinogram at the eye opening stage. These results suggest that human LCA8 can be modeled in the mouse by simultaneously ablating Crb1/2 from the beginning of eye development. Importantly, they also indicate that LCA8 is caused by malfunction of retinal progenitor cells during early ocular development rather than by defective photoreceptor-Muller glial interaction, a mechanism proposed for RP12.

1. Introduction

Crumbs homolog genes (Crb1, Crb2 and Crb3) encode large, single-pass transmembrane proteins that are essential for forming and maintaining apical cell polarity and cell-cell junctions (den Hollander et al., 2008; den Hollander et al., 1999; Quinn et al., 2017). Crumbs proteins, along with two scaffolding proteins, Pals1 (protein associated with lin-seven 1) and Patj (protein associated with tight junction), form the core of the apical Crumbs polarity complex (Assemat et al., 2008; Wang and Margolis, 2007). This is one of two interacting apical polarity complexes in epithelial cells; the other is the Par complex (Assemat et al., 2008; Campanale et al., 2017; Hurd et al., 2003; Tepass, 2012). In developed retina, Crumbs proteins form an apical adhesion belt by homophillic and/or heterophilic interactions of the extracellular domains of Crb1 and/or Crb2 enriched with protein-protein interaction domains situated at the apical surface of the developing retinal epithelium and (Letizia et al., 2013; Meuleman et al., 2004; Quinn et al., 2017; Thompson et al., 2013; van de Pavert et al., 2004): Crb2 localizes at the apical surface of developing retina at E18.5 (Alves et al., 2013a) and Crb1 is abundantly expressed in developing retina at E12.5 (den Hollander et al., 2002). In mature retina, the belt, known as the outer limiting membrane (OLM) or external limiting membrane, is formed between photoreceptors and Muller glial cells (MGCs): Crb1 is exclusively expressed in MGCs while Crb2 is expressed in both MGCs and photoreceptors (van Rossum et al., 2006).

Mutations in these genes are associated with various forms of degenerative retinal diseases, including retinitis pigmentosa 12 (RP12), and Leber congenital amaurosis 8 (LCA8) (Alves et al., 2013b; Cremers et al., 2002; den Hollander et al., 2004; den Hollander et al., 2001; den Hollander et al., 2008; Lotery et al., 2001; Pellissier et al., 2013). RP is a

* Corresponding author. Shriners Hospitals Pediatric Research Center, Department of Anatomy and Cell Biology, Lewis Katz School of Medicine, Temple University, USA.
E-mail address: seo.hee.cho@temple.edu (S.-H. Cho).

https://doi.org/10.1016/j.ydbio.2019.05.008
Received 14 January 2019; Received in revised form 20 May 2019; Accepted 21 May 2019
Available online 28 May 2019

family of degenerative retinal disorders caused by genetic mutations in approximately 80 genes followed by progressive rod photoreceptor loss beginning in childhood or adulthood (Ali et al., 2017; Dias et al., 2018; Farrar et al., 2017; Verbakel et al., 2018)(Facts About Retinitis Pigmentosa. National Eye Institute, May 2014). LCA is a similar group of degenerative photoreceptor diseases that, however, appear at birth or in the first few months of life (Kumaran et al., 2017; Stone, 2007). To date, approximately 20–25 genes are known to cause LCA when homozygously mutated (Chen et al., 2013; Coussa et al., 2017; Kumaran et al., 2017). The electroretinogram (ERG) response of LCA patients is severely attenuated or absent at birth. In RP patients vision loss starts in the periphery and progresses toward the center, leaving only tunnel vision until vision is ultimately lost completely (Shintani et al., 2009). Although mutations in Crb1 genes in humans are responsible for RP12 and LCA8, strong genotype-phenotype correlation is not clear (den Hollander et al., 2004; Khan et al., 2018; Motta et al., 2017), probably because environmental factors and genetic modifiers influence disease severity. It is plausible that complete loss of Crb1 induces LCA8 more frequently than RP12 and that partial loss of function induces RP, however, this idea requires further investigation (den Hollander et al., 2004).

Genes implicated in LCA affect various aspects of photoreceptor cells in several different ways (Chacon-Camacho and Zenteno, 2015; Coussa et al., 2017; Kumaran et al., 2017). First, most of these genes are expressed exclusively or predominantly in the retina or the retinal pigment epithelium (RPE). Second, these genes encode proteins essential for photoreceptor function, including phototransduction, the visual cycle, development and structural maintenance (Astuti et al., 2016; den Hollander et al., 2008; Kumaran et al., 2017). Therefore, the initiation of LCA pathology is gene-specific. Most LCA proteins localizing at subcellular structures are directly required by the photoreceptor cells while several are essential for RPE and indirectly influence photoreceptor survival (Dias et al., 2018; Kumaran et al., 2017). TULP1, CEP290, RPGRIP1, LCA5 and SPATA7 localize at the connecting cilium and are involved in ciliary transport. GUCY2D, AIPL1 and RD3 localize in the outer segment (OS) and are essential for phototransduction. RDH12, LRAT and RPE65 are essential for retinoid cycling in the RPE. IMPDH1 is essential for guanine synthesis in the IS. CRX and GDF6 are essential for photoreceptor morphogenesis. CRB1 localizes solely at the OLM and is essential for cell-cell interactions between retinal progenitor cells in the developing retina and between photoreceptors and MGCs in the mature retina (Pellissier et al., 2013; van Rossum et al., 2006).

Although there are significant variations in severity and rate of progression, patients with LCA8 due to CRB1 mutations have common features, including macular atrophy, nummular pigmentation, paraarteriolar preservation of the RPE, and retinal thickening with loss of distinct lamination such as coarse and abnormal layering (Bujakowska et al., 2012; Ehrenberg et al., 2013; Jacobson et al., 2003; Talib et al., 2017). The latter feature is unique to LCA8; progressive thinning of the retina is common in other forms of LCA (Kumaran et al., 2017). In addition, optical coherence tomography (OCT) reveals intraretinal hyperreflective lesions in LCA8 patients with some resemblance to those in mouse rd8 retinas (Aleman et al., 2011). Whether these structures correspond to pseudorosettes or represent a pathology novel to LCA8 is unknown.

Crb1/Crb2 dKO mutants generated with Chx10-Cre have recently been used to model LCA8 (Pellissier et al., 2013). While retinal pathology and function were uniquely affected, this approach did not effectively remove Crb1/Crb2 genes from early ocular tissues such as RPE and neural retina. For example, retinal pigmentation is unchanged, probably because expression of Cre is restricted in the retina (Rowan and Cepko, 2004). In addition, because the robust onset of Cre protein expression does not begin in subsets of retinal progenitors until E11.5, Crb1/Crb2 gene ablation in retina is delayed (Rowan and Cepko, 2004). Most importantly, it has not been established whether retinal function is attenuated at the eye-opening stage in this mutant.

In this study, we identify genetic conditions that exhibit RP12- or LCA-8-like phenotypes by comprehensive bi-allelic analysis of Crb1 and Crb2. We also demonstrate that complete absence of Crumbs polarity complex (Crb1/Crb2 dKO) during early ocular development causes abnormalities in retinal and RPE progenitor cells that induce distinct phenotypes that closely mimic LC8-like pathologies. In addition, we provide important insights into understanding the compensatory function of Crumbs polarity complex proteins during eye development.

2. Results

2.1. Generation of ocular tissue-specific series of CRB1/2 MUTANTS

In order to investigate the function of Crb1 and Crb2 in ocular development and produce mouse models of LCA8, we generated floxed alleles of Crb1 and Crb2 by *in vitro* fertilization using blastocyst injection (Fox Chase Cancer Center, Laboratory Animal Facility, Temple University) of Crb1-targeted ES cells ($Crb1^{f/+}$) with frozen $Crb2^{f/+}$ sperm, followed by injected implantation into surrogate females (University of Wisconsin, Transgenic Facility) (Supp. Fig. 1). We used mRX-Cre, which permits Cre protein expression in the optic vesicle, which develops into neural retina and RPE at E8.5, to achieve early retina/RPE-specific ablation of Crb1 and Crb2. This ablation overcomes the shortcomings of the previous Crb1/Crb2 dKO using Chx10-Cre driver, which only partially mimics LCA8 pathology (Klimova et al., 2013; Pellissier et al., 2013). Because it is possible that JM8A3.N1, an ES cell line used to target Crb1, harbors the rd8 allele, we genotyped the mice containing Crb1 flox allele with PCR to check for the nucleotide deletion at nt 3481 found in rd8 (Mehalow et al, 2003). Because some mutations, such as rd1, occur commonly in various mouse strains, we also checked for the change found in rd1, a different mutation causing retinal degeneration in FVB/N, another wild type (WT) strain commonly used to generate transgenic mice (Chang et al., 2013; Gimenez and Montoliu, 2001; Mattapallil et al., 2012). All mice carrying one or two loxP sites in a Crb1 gene, $Crb1^{f/+}$ or $Crb1^{f/f}$, contained one or two rd8 mutations, respectively, but not the rd1 allele, in a manner that suggests linkage between the loxP and rd8 alleles. Therefore, genotypes of Crb1 mutants are $Crb1^{f(rd8)/+}$ or $Crb1^{f(rd8)/f(rd8)}$).

We used these flox alleles of Crb1 and Crb2 and an mRX-Cre driver allele to generate multiple bi-allelic combinations: **HET/HET**; $Crb1^{f(rd8)/+}$; $Crb2^{f/+}$; mRX-Cre, **HO/WT (Crb1 cKO)**; $Crb1^{f(rd8)/f(rd8)}$; $Crb2^{+/+}$, **HO/HET**; $Crb1^{f(rd8)/f(rd8)}$; $Crb2^{f/+}$; mRX-Cre, **WT/HO (Crb2 cKO)**; $Crb1^{+/+}$; $Crb2^{f/f}$; mRX-Cre, **HET/HO**; $Crb1^{f(rd8)/+}$; $Crb2^{f/f}$; mRX-Cre and **HO/HO (Crb1/Crb2 dKO)**; $Crb1^{f(rd8)/f(rd8)}$; $Crb2^{f/f}$; mRX-Cre.

2.2. CRB1/CRB2 dKO SHOWS histological defects reminiscent of human LCA8 at the adult stage

Crb1, Crb2, and Crb1/Crb2 mutations in mice have been shown to express a retinal phenotype, such as a break in the OLM manifested by protrusion of ONL cells toward RPE, retinal folding, and rosette formation(Aleman et al., 2011; Alves et al., 2013a, 2014b; Pellissier et al., 2013, 2014). In order to evaluate the effects of Crb1/Crb2 gene dosage on the retinal phenotype and determine whether there are gene- and/or dose-specific structural defects, we first used the Hematoxylin and Eosin (H&E) histological method to examine multiple eyes of each genotype at the adult stage. One important question was to determine whether combinations of Crb1/Crb2 mutations induce quantitative and/or qualitative differences in retinal phenotype.

Compared to WT (n = 7), HET/HET (n = 5) did not show any distinct abnormalities (Fig. 1A and data not shown). HO/WT retinas (n = 2) did not exhibit any obvious phenotype except rare small rosettes or OLM breaks and ONL protrusions that were similar to those of the rd8 allele (Aleman et al., 2011)(Fig. 1B – B"). Some parts of sections from HO/HET (n = 6) and WT/HO (n = 4) retinas showed laminar defects, including rosettes and fusion of inner and outer nuclear layers (INL and ONL), therefore partial absence of inner plexiform layer (IPL) (Fig. 1C and D). HET/HO retinas (n = 6) showed nearly complete absence of ONL, while

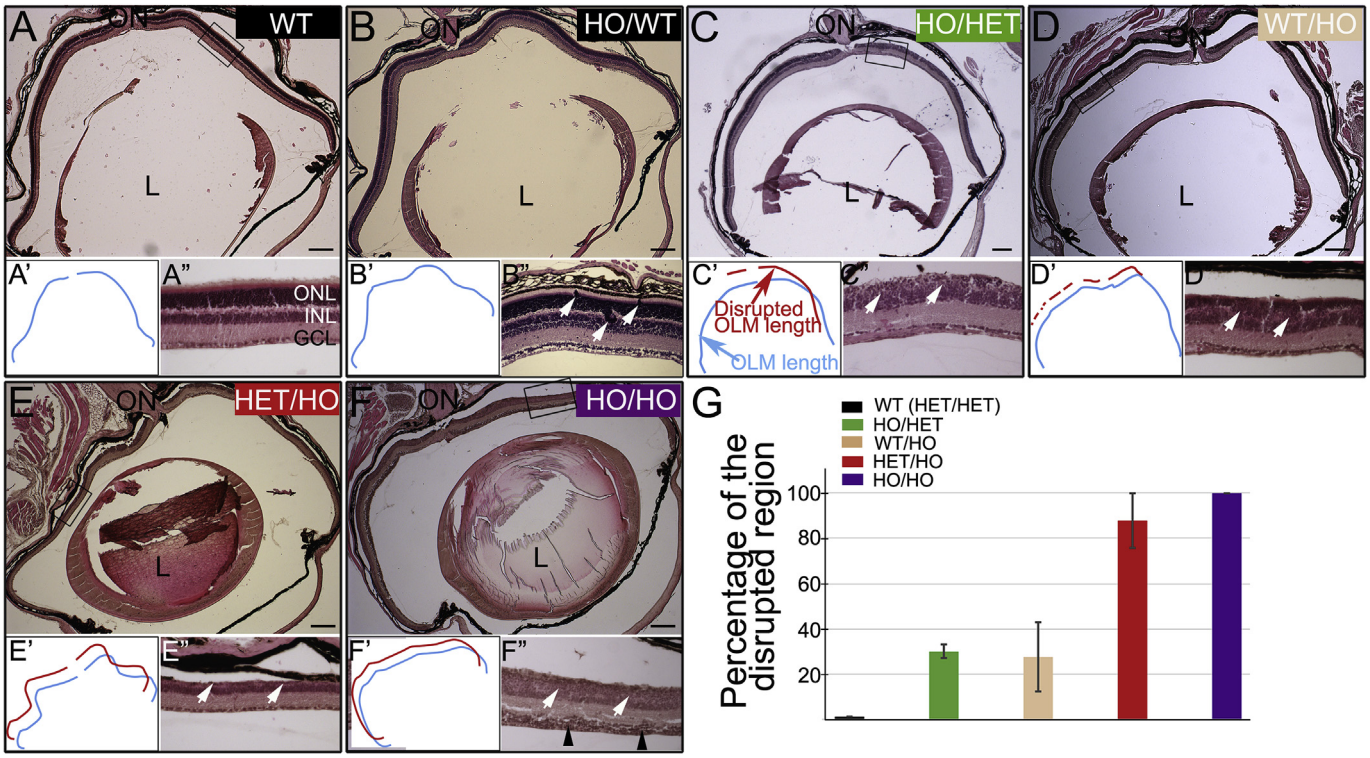

Fig. 1. Crb1/Crb2 mutant series shows dose-dependent retinal dysplasia at adult stage. (A–F) Representative H&E images of WT (A), HO/WT (B), HO/HET (C), WT/HO (D), HET/HO (E), and HO/HO (F) are shown. Tracings of the length of normal (blue line) and dysplastic (red line) OLMs are indicated (A' – F'). Insets represent images at high magnification except B" (A", C" - F"). Image showing rare OLM and lamination defects (white arrows) in B" was stained with H&E at P23. Other lamination defects include absence of OPL, mixing of INL and ONL cells (arrows, C" – F"), and ectopic accumulation of retinal cells in GCL (arrowheads, F"). Scale bar, 100 μm. G. The mean percentages of the normal/defective retinas in WT (black), HO/HET (green), WT/HO (beige), HET/HO (red), and HO/HO (purple) are plotted. L, lens; ON, optic nerve; ONL, outer nuclear layer; INL, inner nuclear layer; GCL, ganglion cell layer.

INL was mildly affected and ganglion cell layer (GCL) generally intact (Fig. 1E). Intriguingly, HO/HO retinas (n = 4) showed thickened GCL, severely diffuse INL (loosely packed), and partially absent ONL (Fig. 1F). Some, but not all, of the thickened GCLs contained an increased number of cells. In contrast to WT retinas, where the GCL consisted of a row of cells uniformly staining pale pink, the GCL of HO/HO retinas comprised a mixture of cells staining pale and dark purple. Cells showing a similar heterogeneity of shades of purple were also present in the upper layer: the presence of subsets of cells staining either dark purple or pale purple suggested severe disruption of retinal lamination. Retinal rosettes with variable size and disrupted/absent OLM were observed in the mutant series except HET/HET. Intriguingly, round spots or patches devoid of retinal cells that are different from retinal rosettes also appeared on the apical surface of HO/HO retinas and rarely in HET/HO, but not in WT/HO or HO/WT (Fig. 1; see Fig. 6 for detailed analysis).

We next assessed the extent of the retinal abnormalities in this series of mutants at the adult stage. Briefly, for straightforward quantification of the retinal defects, we calculated the percentage of the lesion from measurements of the length of OLM overarching the defective retinal area and total OLM length (% lesion = OLM length (overarching defective retina, red lines in Fig. 1)/OLM length (total, blue lines) X 100). Because HET/HET and HO/WT did not show a measurable degree of the phenotype, they were excluded from this assay. Fig. 1G shows that there was a gradual increase of defects compared to WT: HO/HET (n = 5) and WT/HO (n = 3) showed 30.1 ± 6.5 and 27.4 ± 26.4%, respectively; HET/HO (n = 5) and HO/HO (n = 3) showed widespread lesions over the entire retina (87.8 ± 26.7% and 100 ± 0%, respectively). In general there was a degree of phenotypic variation in HO/HET, WT/HO and HET/HO retinas, whereas HO/HO retinas showed 100% penetrance. In summary, there was quantitative difference among members of the Crb1/Crb2 mutant series. For example, weak alleles, such as deletion of two copies of the Crb1 gene (HO/WT) or one copy of Crb1 and Crb2 (HET/HET), did not show a measurable phenotype. Deletion of two copies of the Crb2 gene (WT/HO) or two copies of the Crb1 gene and one copy of Crb2 (HO/HET) induced a moderate phenotype, while strong alleles, such as deletion of two copies of Crb1 and Crb2 (HO/HO) or one copy of Crb1 and two copies of Crb2 (HET/HO), elicited a severe phenotype. In addition, histological study showed that only the strong allele deleting both copies of Crb1 and Crb2 (HO/HO) induced unique laminar defects that were qualitatively different from those of other allelic combinations, where the extent of the ONL rosettes differed.

2.3. *CRB1/CRB2 DKO and HET/HO mutants SHOW severely reduced Electroretinography responses at the adult stage*

Electroretinography has been an informative assay for evaluating eyes with inherited retinal dystrophies. In general, a- and b-wave amplitudes are severely reduced and a- and b-wave latencies delayed in RP, whereas responses are nearly extinguished in LCA patients and LCA mouse models (Alves et al., 2014a; Foxman et al., 1985; Hamasaki et al., 2002; Mookherjee et al., 2015; Pellissier et al., 2013). Because photoreceptor cells determine the latency of the a-wave under both scotopic and photopic conditions, altered latency in RP patients suggests that rods and cones are affected in significant areas of the retina (Hamasaki et al., 2002; Qiu et al., 2002).

In order to assess the retinal function of the Crb1/Crb2 mutants at the adult stage, we studied the ERG in multiple mice of each genotype (Fig. 2). Photoreceptor functions were assessed by determining the peak latency (time measured from the onset of the flash to the response peak) and amplitude of the a-wave after dark-adaptation (scotopic) (Fig. 2A – F); cone function was specifically assessed by determining b-wave amplitude after adaptation to light (photopic) (Fig. 2A' - F'). The function

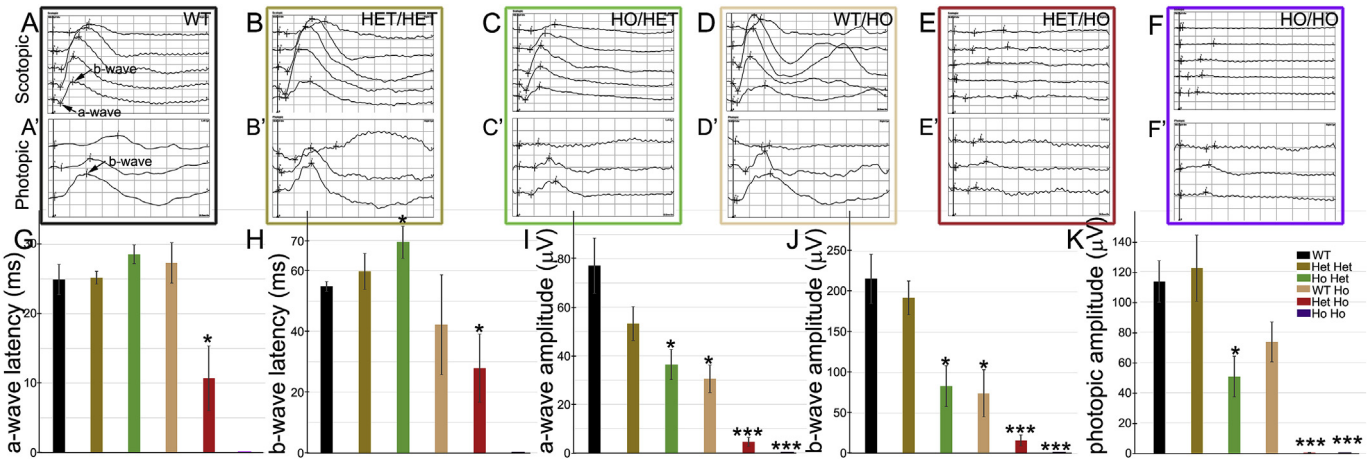

Fig. 2. Severely attenuated or nearly absent ERG responses in Crb1/Crb2 (HET/HO) and Crb1/Crb2 dKO (HO/HO). (A – F′) Representative electroretinograms of WT (A & A′), HET/HET (B & B′), HO/HET (C & C′), WT/HO (D & D′), HET/HO (E & E′), and HO/HO (F & F′) after dark- (A–F) and light- (A' – F′) adaptations. (A–F) Five traces represent scotopic ERG responses to varying input flash light intensities ranging from 0.001, 0.01, 0.1, 1, and 10 (cd·s/m^2, from the bottom to top). (A' – F′) Three traces represent photopic ERG responses to three varying input flash intensities from 0.1, 1, 10 (cd·s/m^2, from the bottom to top). (G–K) Quantification of the a-wave peak latency (G), b-wave peak latency (H), a-wave amplitude (I), b-wave amplitude (J), and photopic b-wave amplitude (K) in WT (black), HET/HET (yellow), HO/HET (green), WT/HO (beige), HET/HO (red), and HO/HO (purple) (mean ± SD) at adult stage. *p < 0.05; **p < 0.01; ***p < 0.001 Crb1/Crb2 mutants vs. WT mice, Student's t-test.

of cells in the INL (predominantly ON-bipolar and MG cells) was assessed by the peak latency and amplitude of the b-wave after dark adaptation.

a-wave peak latency was severely altered in HET/HO and HO/HO mice (Fig. 2G; WT mean = 24.94 ± 7.55 ms (n = 10); HET/HET mean = 25.19 ± 2.60 ms (n = 8); HO/HET mean = 28.58 ± 4.28 ms (n = 10); WT/HO mean = 27.32 ± 5.82 ms (n = 6); HET/HO mean = 10.69 ± 17.42 ms (n = 14); HO/HO unidentifiable peak (n = 8)). b-wave peak latency was also significantly altered in HET/HO and HO/HO (Fig. 2H; WT mean = 54.79 ± 5.72 ms (n = 10); HET/HET mean = 59.78 ± 16.74 ms (n = 8); HO/HET mean = 69.37 ± 16.68 ms (n = 10); WT/HO mean = 42.13 ± 32.97 ms (n = 6); HET/HO mean = 27.9 ± 41.92 ms (n = 14); HO/HO unidentifiable peak (n = 8)). Scotopic a-wave amplitudes were significantly decreased in HO/HET, WT/HO, HET/HO and HO/HO (Fig. 2I; WT mean = 77.14 ± 39.53 μV (n = 10); HET/HET mean = 53.28 ± 19.71 μV (n = 8); HO/HET mean = 36.37 ± 19.80 μV (n = 10); WT/HO mean = 30.47 ± 11.36 μV (n = 6); HET/HO mean = 4.48 ± 6.85 μV (n = 14); HO/HO unidentifiable peak (n = 8)). Scotopic b-wave amplitudes were also severely decreased in HO/HET, WT/HO, HET/HO and HO/HO (Fig. 2J; WT mean = 216.05 ± 106.05 μV (n = 10); HET/HET mean = 192.63 ± 59.51 μV (n = 8); HO/HET mean = 83.41 ± 80.37 μV (n = 10); WT/HO mean = 74.47 ± 58.41 μV (n = 6); HET/HO mean = 16.21 ± 25.26 μV (n = 14); HO/HO unidentifiable peak (n = 8)). Photopic b-wave amplitudes were similarly reduced in HO/HET, HET/HO and HO/HO (Fig. 2K; WT mean = 113.44 ± 47.53 μV (n = 10); HET/HET mean = 122.3 ± 61.86 μV (n = 8); HO/HET mean = 50.68 ± 38.00 μV (n = 8); WT/HO mean = 73.55 ± 18.58 μV (n = 4); HET/HO mean = 0.33 ± 0.77 μV (n = 14); HO/HO unidentifiable peak (n = 8)). These analyses demonstrate a dose-dependent reduction of scotopic ERG responses (altered a- and b-wave amplitudes) in the Crb1/Crb2 mutant series.

2.4. CRB1/CRB2 DKO and HET/HO mutants SHOW severely reduced optokinetic responses at the adult stage

The attenuated ERG responses suggest that the Crb1/Crb2 mutations severely compromise visual function. To assess the effects on visual function, we studied optokinetic responses under photopic conditions with the OptoMotry system, a behavioral test that determines visual acuity and contrast sensitivity of the mice (Fig. 3A; CerebralMechanics (Lethbridge, Canada)) (Ku et al., 2015; Prusky et al., 2004; Zulliger et al., 2011). Acuity is quantitated by the maximal threshold spatial frequency of the gratings that induces a head-tracking reflex (Kolesnikov et al., 2010); higher maximal frequencies suggest greater visual acuity. Adult HET/HET, HO/HET, and WT/HO mice showed significantly reduced maximal threshold spatial frequencies compared to WT (Fig. 3B; WT

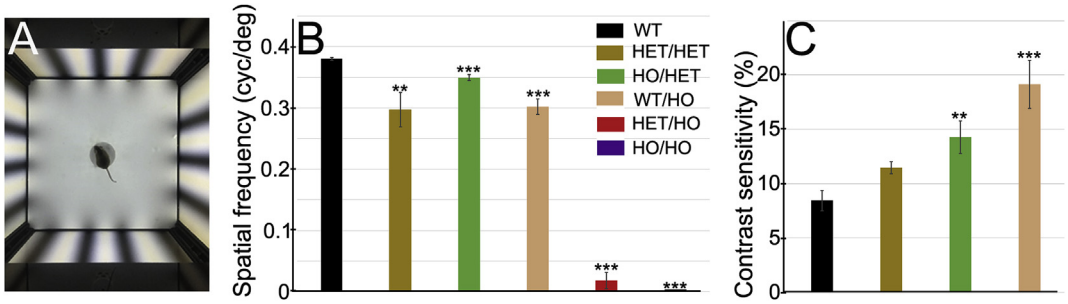

Fig. 3. Severely attenuated optokinetic responses (visual acuity and contrast sensitivity) in Crb1/Crb2 (HET/HO) and Crb1/Crb2 dKO (HO/HO). (A) Image showing the arrangement of the 4 monitors, generating cylinder grating, and central platform where a single mouse tracks the drifting gratings with head and neck movement (Prusky et al., 2004). (B & C) Quantification of the optokinetic responses of the Crb1/Crb2 mutant series measuring maximal spatial frequencies (visual acuity (cyc/deg, B) and contrast sensitivity (%, C) under photopic conditions at adult stage. *p < 0.05; **p < 0.01; ***p < 0.001 Crb1/Crb2 mutants vs. WT mice, Student's t-test.

mean = 0.38 ± 0.01 cyc/deg (n = 12); HET/HET mean = 0.39 ± 0.08 cyc/deg (n = 6); HO/HET mean = 0.35 ± 0.01 cyc/deg (n = 8); WT/HO mean = 0.30 ± 0.04 cyc/deg (n = 6)). The decrease was even greater in HET/HO and HO/HO (HET/HO mean = 0.02 ± 0.05 (n = 12); HO/HO response unidentifiable (n = 8)). We also determined the threshold of the contrast sensitivity of the mice at a spatial frequency of 0.2 cyc/deg. Because HET/HO and HO/HO did not show any optokinetic responses at this frequency, they were omitted from this test. Compared to WT (8.45 ± 3.0% (n = 10)), HET/HET, HO/HET and WT/HO showed statistically decreased sensitivity (Fig. 3C; HET/HET mean = 11.45 ± 1.34% (n = 4); HO/HET mean = 14.28 ± 4.30% (n = 8); WT/HO mean = 19.12 ± 4.42% (n = 6)). These results are consistent with the ERG data and indicate that visual function is severely impaired in HO/HO and HET/HO mice and partially lost in the other mutants, including HET/HET, HO/HET, and WT/HO.

2.5. CRB1/CRB2 DKO retinas demonstrate central thickening at P21

One of the most striking features that OCT reveals about human LCA8 patients is thickened retinal morphology around the optic nerve (Aleman et al., 2011; Jacobson et al., 2003). In order to determine whether there is thickening of the retina in the Crb1/Crb2 mutants, we measured epithelial thickness in paraffin sections obtained from central, optic disc-containing retinal regions of WT, HET/HO, and HO/HO mutant eyes. Because the retinal phenotype was weaker in HET/HET, HO/HET, and WT/HO, these lines were excluded from this analysis. Instead, we compared HO/HO and HET/HO mice, in which retinal disorganization was the most severe, to WT. We measured the thickness at 6 equally-spaced locations in both halves of the retina (12 locations per retina), avoiding the optic disc, and plotted the results as shown (Fig. 4A). To examine progression at early, intermediate, and late stages of the disease, measurements were made and compared with control WT littermates at three time points, P0, P21 and adult (Fig. 4B – D). At P0, retinal thickness was not significantly different from WT at any of the 12 positions (n = 9: HET/HO, n = 5; HO/HO, n = 4) (Fig. 4B). At P21, the Crb1/Crb2 (HO/HO) retinas (4G and G′, means = 204.6 and 202.0, n = 5) were significantly thicker than WT (4E and E′, means = 156.1 and 156.6, n = 7) and HET/HO (4F and F′, means = 165.8 and 181.0, n = 5) at two central locations flanking the optic disc (Fig. 4C and E – G'). In HO/HO retinas we frequently observed accumulated cells in the GCL (arrows) in areas flanking these locations and disorganization, including lack of INL and ONL separation and absence of outer plexiform layer (OPL), was prevalent throughout. Acellular spots were also more frequent (arrowheads) and they localized preferentially in the central retina surrounding the optic disc. At the adult stage, all regions of HET/HO retinas (n = 8) were significantly thinner than those of WT (n = 5), whereas HO/HO retinas (n = 5) were generally thinner than those of WT, but significantly different at one central position (HO/HO mean = 108; WT mean = 130.4) and two peripheral positions (HO/HO means = 68.5 and 67.4; WT means = 82 and 98.4, respectively) (Fig. 4D).

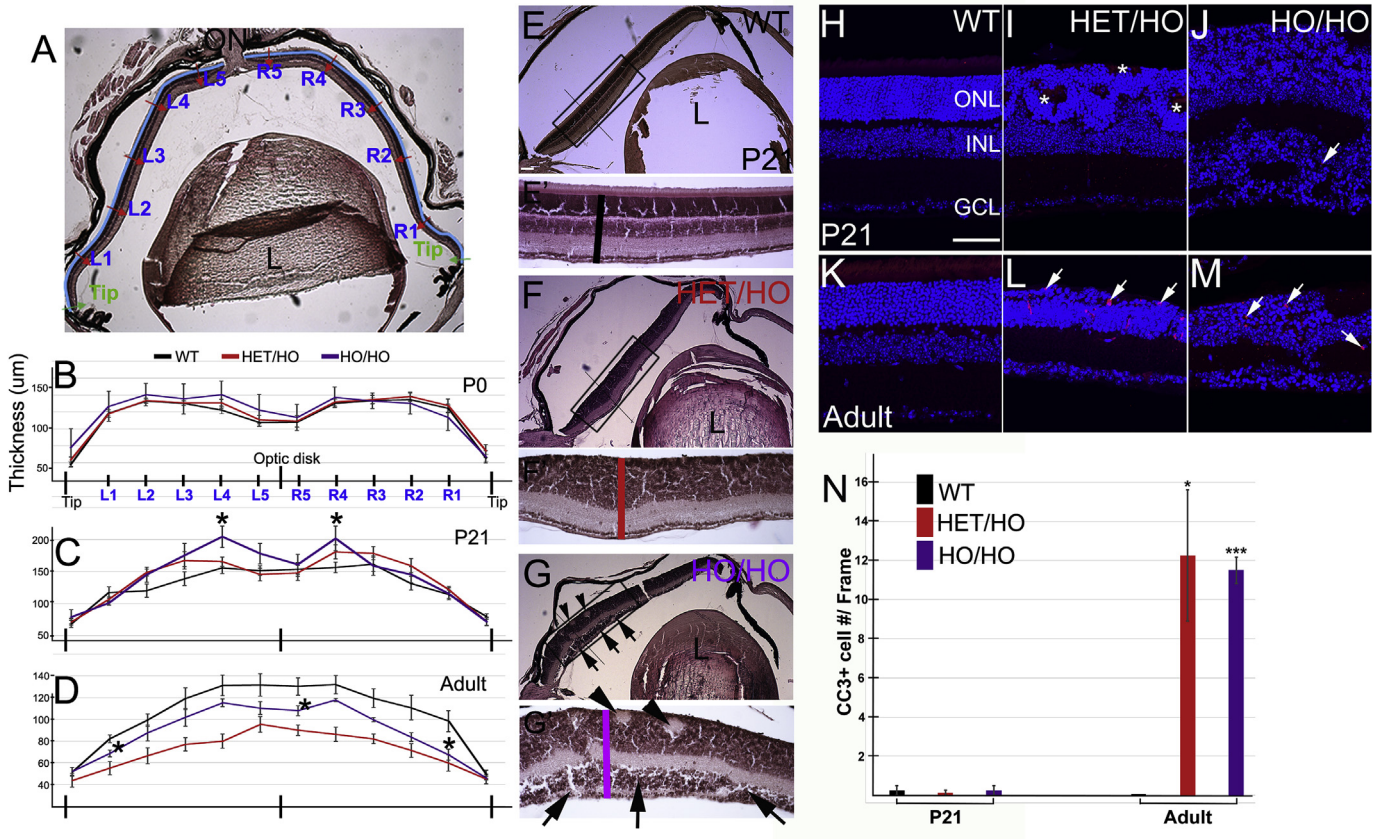

Fig. 4. Localized retinal thickening in Crb1/Crb2 dKO (HO/HO). (A) Representative image showing the length of OLM of each retinal leaflet half, and the intervals and locations of the retina where thickness was measured. L1 – L5 represent 5 equally spaced positions in the left half of the retina and R1 – R5 represent positions from the right half. Measurements at the retinal tips were made at locations 25 mm away from the ora serrata. (B–D) Quantification of retinal thickness of Crb1/Crb2 (HET/HO) and (HO/HO) compared to WT (mean ± SD) at P0 (B), P21 (C), and adult stage (D). *p < 0.05; **p < 0.01; ***p < 0.001 Crb1/Crb2 mutants vs. WT mice, n > 5 per group, Student's t-test. (E – G′) Representative histological images of retinas used for the thickness measurements at P21 from WT (E and E′), HET/HO (F and F′) and HO/HO (G and G′). Lines indicate the positions where the measurements were made, such as L4 or R4. Scale bar, 100 μm. (H–M) α-Cleaved caspase 3 staining (arrows) of WT (H & K), HET/HO (I & L), and HO/HO (J & M) at P21 (H–J) and adult stages (K–M). * indicates auto-fluorescence from the outer segments. (N) Quantification of α-CC3+ cells in WT, HET/HO, and HO/HO retinas at P21 and adult. *p < 0.05; ***p < 0.001 Crb1/Crb2 mutants vs. WT mice, n > 4 per group, Student's t-test. L, lens; ON, optic nerve, ONL, outer nuclear layer; INL, inner nuclear layer; GCL, ganglion cell layer; tip, retinal tip.

These results indicate that at P21 retinas of HO/HO, but not of HET/HO, mice model the severely thickened central retinal morphology frequently observed in human LCA8 patients. In addition, the thickness measurements at the adult stage, taken together with the histology results, indicate the loss of a significant number of cells in HET/HO and HO/HO retinas.

To determine whether caspase 3- dependent apoptosis plays an important role in cell loss in Crb1/2 mutant, we immunostained for activated caspase 3 (cleaved caspase 3, CC3) at P21 (n = 8, each) and adult stages (n = 4 for WT and HET/HO and n = 8 for HO/HO) (Fig. 4H – M). CC3+ cells were rare in any of the three conditions at P21, but dramatically increased compared to WT in HET/HO and HO/HO retinas at adult stages (Fig. 4N).

2.6. CRB1/CRB2 DKO retinas SHOW near-random distribution of photoreceptors at P0 and P21

The morphological defects that we observed in H&E stained preparations, including irregular, mosaic cellular distribution; thickened GCL; and loosely packed INL cells, suggest that postmitotic retinal cells are likely to be abnormally positioned during development in the HO/HO retinas. To test this possibility, we examined the distribution of rod photoreceptor cells in developing (P0) and mature (P21) retinas (Fig. 5). Staining with α-Rhodopsin antibody revealed that newly differentiated, immature rod cells with bipolar morphology normally appeared at the apical (scleral) surface of the retinal epithelium at P0, where they were positioned perpendicular to the OLM, which we stained for pan-Crb (Fig. 5A and D). In the affected regions of HET/HO retinas, immature rod cells localized perpendicularly to the fragmented and/or disrupted OLM within rosettes, half-rosettes, and foldings, which maintained their apical localization (Fig. 5B and E). However, immature rod cells were randomly distributed in the outer neuroblastic layer (ONBL) of HO/HO retinas, which pan-Crb staining revealed to have lost apical tissue polarity (Fig. 5C and F). Remarkably, some rod cells were located in the thickened inner neuroblastic layer (INBL), suggesting that they had been displaced ectopically to the basal (vitreal) surface. In order to quantify the degree of dislocation, we determined the precise distribution of the newly formed rod cells within sectors of the retinal epithelium at P0. We divided the retinal epithelium into 4 bins: 3 were in the ONBL; the 4th corresponded to IPL and INBL. In WT retinas, the entire population of newly formed rod cells was located in the top bin (Fig. 5G). In HET/HO and HO/HO retinas, increasing fractions were located in the lower bins. In HET/HO retinas, 63 ± 17.7% were localized in the top bin, 32 ± 13.5% were in bin #2, and 4.1 ± 1.1% were in bin #3. Rare rod cells were also localized in the lowest bin. In HO/HO retinas, 48 ± 11.7% were localized in the top bin, 26.4 ± 7.3% in bin #2, and 15.2 ± 4.7% in bin #3. Remarkably, 10.3 ± 6.8% of α-Rhodopsin + cells were displaced to the lowest bin.

To determine rod cell distribution at maturity, we divided the retina into 3 bins and carried out a similar analysis at P21 (Fig. 5H – M and N). In WT, α-Rhodopsin staining revealed that rod cells were exclusively located within ONL; staining was weak in the ONL, strong in the OS (Fig. 5H and K). In HET/HO retinas, weak staining remained and formed rosettes in the disrupted ONL; strong staining, which represented fragmented OS, appeared in the inner space of the rosettes (Fig. 5I and L). In HO/HO retinas, rod cells were no longer positioned only at the apical side (Fig. 5J and M). Instead, rod cells were ectopically distributed in the lower portions of the retinal epithelium: 63 ± 6.9% rod cells remained in the top bin, 12.1 ± 2.4% in bin #2, and 24.1 ± 4.5% in bin #3. In rare cases of HET/HO retinas, rod cell distributions at P0 and P21 were similar to those of HO/HO, which were excluded due to rarity. These results suggest that dislocation of retinal cells is responsible for the indistinct layering found in HO/HO retinas.

2.7. CRB1/CRB2 DKO retinas SHOW spots at P0 and P21 that differ from rosettes frequent in CRB1- and CRB2-DEFICIENT retinas

One prominent histological feature of the HO/HO and HET/HO

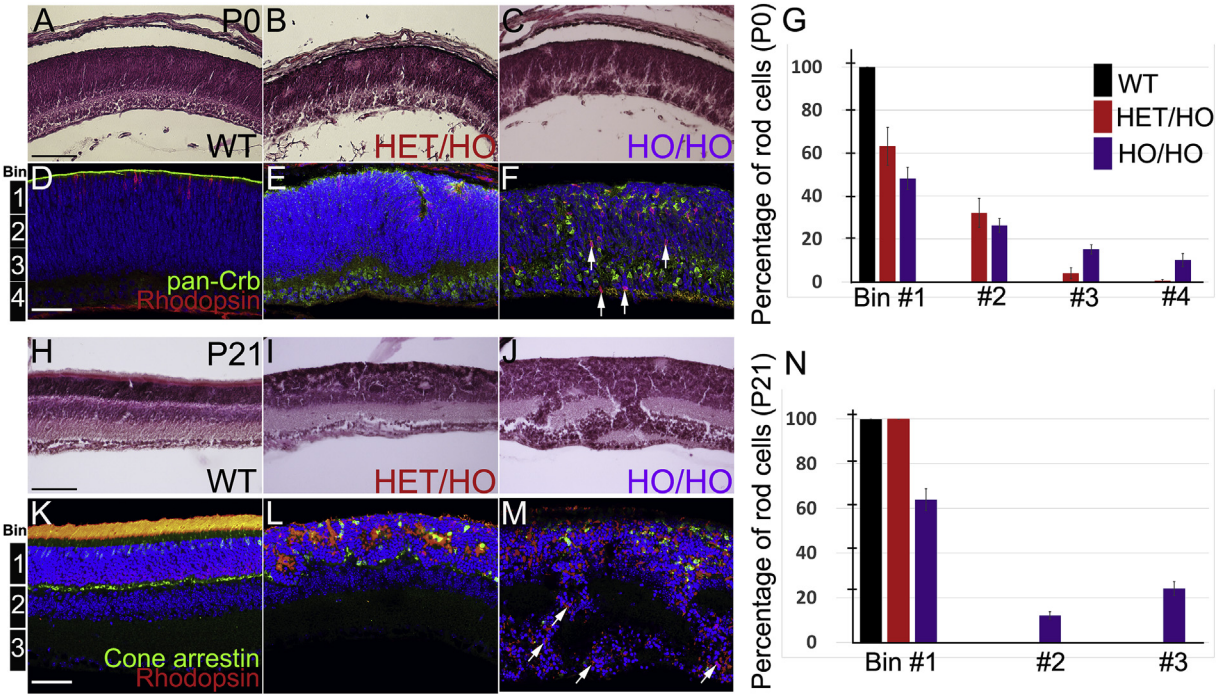

Fig. 5. Rod photoreceptor cells are abnormally distributed (basally dislocated) in Crb1/Crb2 (HO/HO) retinas at both P0 and P21. (A–F) H&E staining and IF staining with α-Rhodopsin (red) and α-pan-Crb (green) of WT (A & D), HET/HO (B & E), and HO/HO (C & F) at P0. (G) The distributions of rod cells in 4 bins are plotted. (H–M) H&E staining and IF staining with α-Rhodopsin (red) and α-cone arrestin (green) of WT (H & K), HET/HO (I & L), and HO/HO (J & M) at P21. (N) The distributions of rod cells in 3 bins are plotted. Examples of abnormally displaced rod cells are marked (arrows in F and M). Scale bars, 100 μm (A – C and H - J) and 50 μm (D – F and K – M).

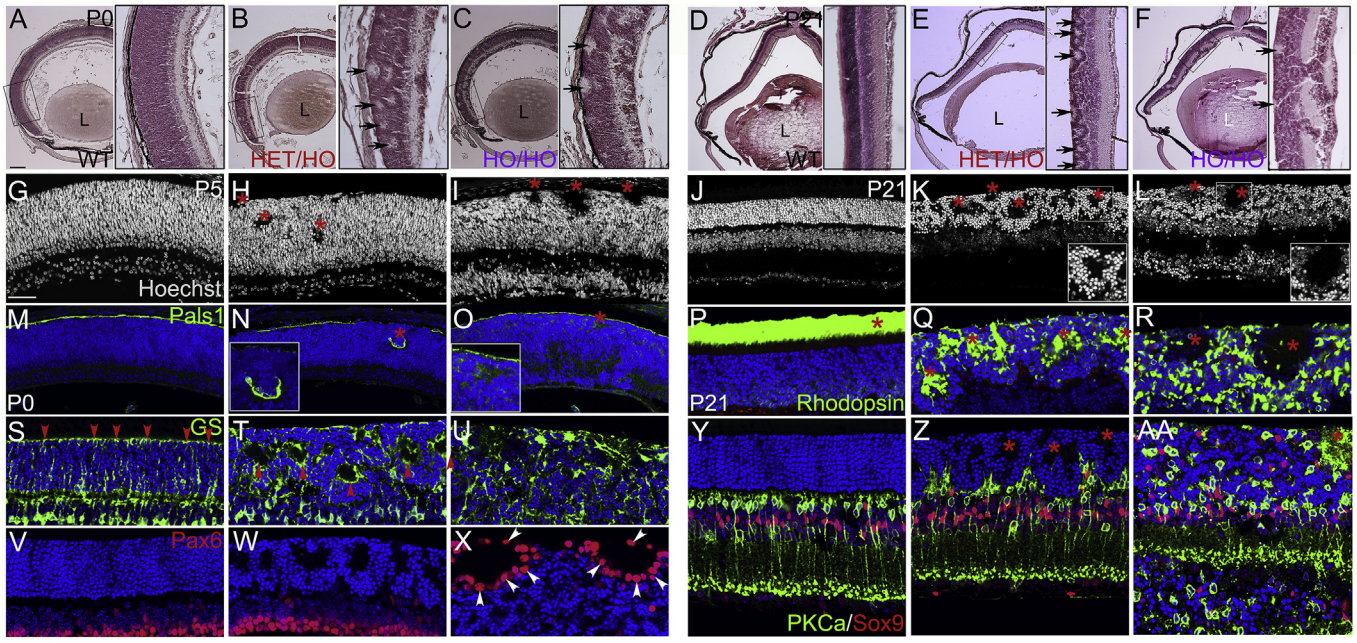

Fig. 6. Crb1/Crb2 dKO (HO/HO) retinas show unique retinal spots that are distinct from rosettes commonly observed in Crb1-deficient retinas. (A–F) H&E staining of WT (A & D), HET/HO (B & E), and HO/HO (C & F) shows spots (arrows) lacking retinal cells at P0 (A–C) and P21 (D–F). (G–L) Staining with Hoechst dye also shows spots (asterisks) in HET/HO and HO/HO at P5 (G–I) and P21 (J–L). (M–O) α-Pals1 staining is disrupted and/or severely reduced in HET/HO (N) and HO/HO (O) compared to WT (M). Pals1 signal in or around spots (asterisks and insets) is absent in HO/HO (O) but not in HET/HO (N). (P–R) Normal Rhodopsin signal in the OS of photoreceptor cells (asterisk, P) is included in the spots of HET/HO (Q) but not of HO/HO retinas (R). (S–U) Apical α-GS (green) marking MG endfeet in the WT (S) is present in the edges of the spots in HET/HO (T), but absent in HO/HO (U). (V–X) Empty spots in the HO/HO are surrounded by Pax6+ cells. Positioning of Pax6+ cells in the inner nuclear layer is not disturbed in HET/HO (W) compared to WT (V). However, Pax6+ cells surround the empty spots in HO/HO (X). (Y –AA) Inside of the empty spots is filled with the processes of the retinal cells. Compared to the WT (Y), PKCa + bipolar cells are apically localized (Z). In HO/HO (AA), Pax6+ processes are fills the inside of the empty spots. Scale bars, 100 μm (A–F) and 50 μm (G – AA). L, lens.

retinas is retinal spots resembling retinal rosettes or half-rosettes commonly found in Crb1 mutant retinas (Aleman et al., 2011; Coscas et al., 2013; Turgut and Yildirim, 2015). To characterize these spots, we analyzed them histologically at P0 and P21 (Fig. 6A–F). They were preferentially, but not exclusively, located on the apical side of developing and mature retinas. Their size was variable, and their inner portions contained no, or a small number of cells (Fig. 6B, C, E and F). In mature HET/HO retinas they resembled typical retinal rosettes that are surrounded by photoreceptor cells staining dark purple in H&E preparations, but their appearance in HO/HO retinas differed. In order to determine whether these spots in HO/HO retinas were rosettes, we stained retinal sections with Hoechst dye at P5 and P21, when ONL cells can be identified based on their brightness compared to other retinal cells (Fig. 6G – L). In WT, ONBL cells at P5 and ONL cells at P21 had a single very large central chromocenter, and other INBL and INL/GCL cells had several (usually 6–7) small chromocenters adjoining the nuclear periphery or nucleolus (Solovei et al., 2009) (Fig. 6G and J). Careful examination revealed that HO/HO spots were not solely surrounded by ONL cells at P5 and P21, whereas spots in HET/HO retinas (Fig. 6H and K) were surrounded by brightly stained photoreceptor cells and less brightly stained INL cells that were not severely altered. Most cells surrounding the spots in HO/HO retinas were not ONL cells although a small number of ONL cells were present in the vicinity (Fig. 6I and L). This result suggests that the spots in HO/HO retinas are not the retinal rosettes frequently found in Crb1 mutant retinas.

In order to further characterize these spots, we studied HET/HO and HO/HO retinas by IF and compared them to WT at P0 and P21. We first used staining with α-Pals1 antibody to determine whether the spots in HO/HO retinas at P0 were enclosed by a fragmented adhesion belt formed by Crumbs polarity complex (Fig. 6M–O). Unlike HET/HO retinas, in which fragmented adhesion belts were found in the center of rosettes, the spots in HO/HO retinas did not contain α-Pals1+ apical cell-cell adhesions at P0 (Fig. 6N and O). We next used α-Rhodopsin staining to test whether the inner portion of the spots was filled with disrupted OS, as in rosettes induced by Crb1 mutation. Unlike retinas of WT, in which the Rhodopsin signal was strong in the normal OS, and of HET/HO, in which the Rhodopsin signal was strong in the disrupted OS within the rosettes, Rhodopsin signal was not detectable in the spots of HO/HO retinas at P21 (Fig. 6P–R). We then stained with α-GS, a MGC marker, to determine whether the spots were surrounded by Muller glial endfeet. Apical endfeet of MGCs formed a normal OLM in WT retinas at P0 and a disrupted OLM in the rosettes of HET/HO retinas (Fig. 6S and T). However, the array of the GS + endfeet (OLM) did not form a clear adhesion belt in the spots of HO/HO retinas (Fig. 6U). To learn whether the spots were surrounded by non-ONL cells, we studied the location of INL/GCL cells after staining with α-Pax6, a specific marker for amacrine, ganglion, and horizontal cells. Interestingly, α-Pax6+ cells surrounded the spots in HO/HO retinas at P0, but not the rosettes in HET/HO retinas (Fig. 6V–X). Also, processes of PKCα+ bipolar cells were abundant in the spots of HO/HO retinas at P21, but not in the rosettes of HET/HO retinas (Fig. 6Y – AA). These data indicate that retinal spots in HO/HO differ from rosettes in HET/HO; they lack a cell-cell adhesion belt, are not surrounded by photoreceptors, and their inner space is uniquely filled with retinal processes but not photoreceptor OS.

2.8. CRB1/CRB2 dKO, but not HET/HO, mutants SHOW severely attenuated ERG responses at P14 – P16

Histological and IF assays indicated that HO/HO and HET/HO mutants undergo dissimilar disease processes although they share a terminal phenotype: at the adult stage both lack ERG activity and their retinal morphology is thinned. For example, only HO/HO retinas exhibited thickened retinal morphology at P21, severely disrupted cell distribution at P0 and P21, and retinal spots differing from the rosettes and

pseudorosettes common in RP12. Based on these findings, we reasoned that HET/HO might represent a severe form of RP12 and HO/HO exemplify LCA8. These mutant retinas might be structurally and functionally indistinguishable at late phases of disease because progressive retinal degeneration causes structural alterations and functional deficits at adult stages. However, HO/HO retinas might undergo distinct pathological processes during development and early maturity. If so, then the HO/HO, but not the HET/HO, mutant, should lose vision at an early stage, which is a hallmark of LCA8. In order to test this idea, we studied the ERG at P14/P15/P16, when the eyes open and visual function can be assessed for the first time without surgical manipulation. As shown in Fig. 7, scotopic b-wave (means = 76.2 ± 38.4 (WT, n = 6) and 61.7 ± 20.6 (HET/HO, n = 6)) and photopic b-wave amplitude (means = 45.0 ± 20.7 (WT, n = 6) and 37.4 ± 17.2 (HET/HO, n = 6)) were statistically indistinguishable in WT (n = 6) and HET/HO (n = 6) mice, although scotopic a-wave amplitude was significantly reduced in HET/HO (means = 49.6 ± 19.9 (WT, n = 6) and 14.3 ± 8.5 (HET/HO, n = 6)) (Fig. 7A, B, D – F). In contrast, ERG responses were nearly absent in HO/HO mice (n = 6) under both scotopic (mean scotopic a- and b-wave amplitudes = 4.8 ± 5.0 and 20.1 ± 18.5, respectively) and photopic conditions (mean b-wave amplitude = 10.0 ± 15.7) (Fig. 7C, D – F). These data indicate that, at the eye opening stage, HO/HO mice most faithfully recapitulate the severely attenuated visual function of LCA8 patients, which is one of the most prominent features of this disease.

2.9. CRB1/CRB2 DKO, but not HET/HO, mutants display early onset retinal and RPE defects

Defective ocular pigmentation, another hallmark of LCA8, is often manifested as clumped bone spicule pigment, nummular clumps of pigment, or salt-and-pepper retinal pigmentation (Ehrenberg et al., 2013). Consistent with this observation, both mRNA and protein forms of Crb2 are identified in RPE cells (Paniagua et al., 2015; van den Hurk et al., 2005), in which Crb2 proteins are restricted to the apicolateral membrane and co-localize with another Crumbs polarity complex protein Pals1 in tight junctions. In addition, Crb2 mutations in humans induce RPE degeneration by accelerating the epithelial-mesenchymal transition (Chen et al., 2019). A previous LCA8 mouse model using Crb1/Crb2 mutations with Chx10-Cre did not show any changes in retinal pigmentation, presumably because restricted Cre expression in the retina left RPE cells undisturbed (Rowan and Cepko, 2004). Because the mRX-Cre Cre driver used in the present study permits Cre-mediated gene-ablation in developing RPE as well as in the early neural retina (Klimova et al., 2013), we were able to examine pigmentary changes in the retina/RPE and determine whether there was retinal laminar disorganization as early in embryogenesis as E12.5 (Fig. 8). We first confirmed effective ablation of Crb1/Crb2 by α-pan-Crb staining (Fig. 8D – F). Both WT retina and the lens vesicle of HET/HO and HO/HO, where Cre proteins are not expressed, served as internal controls (arrows). α-pan-Crb signal was nearly absent in the apical surfaces of retina/RPE in HO/HO retinas and partially decreased in HET/HO, compared to WT (arrowheads). Histologic examination revealed that, unlike WT and HET/HO, HO/HO eyes contained RPE regions without pigmentation (bracket and arrowheads, Fig. 8A–C, n = 4). Intriguingly, lamination was also severely disturbed in the adjacent retina of these eyes, indicating that the onset of the retinal phenotype was earlier than E12.5 in HO/HO mutant. Taken together, these results therefore suggest that HO/HO mice mimic not only the early-onset retinal defects of human LCA8 but also the pathologies that originate in RPE.

3. Discussion

LCA represents the most severe form of the hereditary retinal dystrophies with vision impairment usually present at birth (Chacon-Camacho and Zenteno, 2015; Coussa et al., 2017; den Hollander et al., 2008; Kumaran et al., 2017). LCA8, which is caused by Crb1 mutations, is one of ~25 types of LCA, and accounts for ~10% of total LCA cases. It is unique among retinal disorders because Crb1 is required for two critical structural functions: maintaining cell adhesions between retinal progenitor cells in the developing retina and photoreceptors and MGCs in

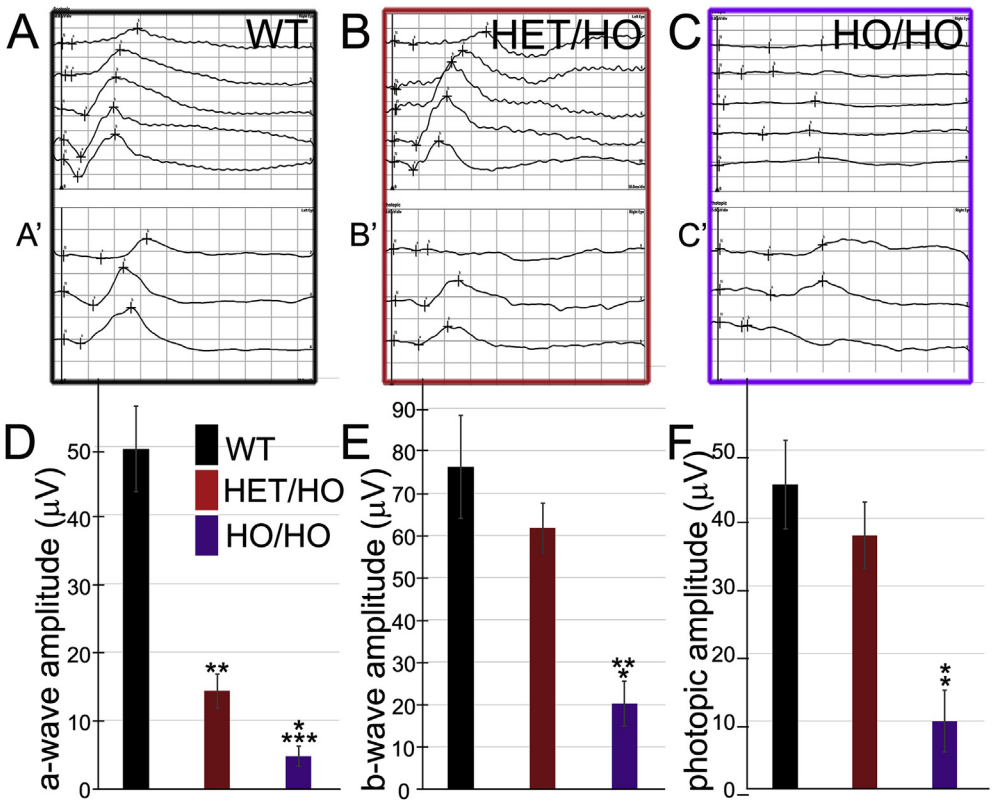

Fig. 7. Crb1/Crb2 dKO (HO/HO) mice are visually impaired at the eye opening stage. (A - C′) Representative electroretinograms of WT (A & A′), HET/HO (B & B′), and HO/HO (C & C′) after dark- (A–C) and light- (A' - C′) adaptations. (D–F) Quantification of scotopic a-wave (D), scotopic b-wave (E), and photopic b-wave (F) amplitudes in WT (black), HET/HO (red), and HO/HO (purple) (mean ± SD) at P14/P15/P16. *p < 0.05; **p < 0.01; ***p < 0.001 Crb1/Crb2 mutants vs. WT mice, Student's t-test.

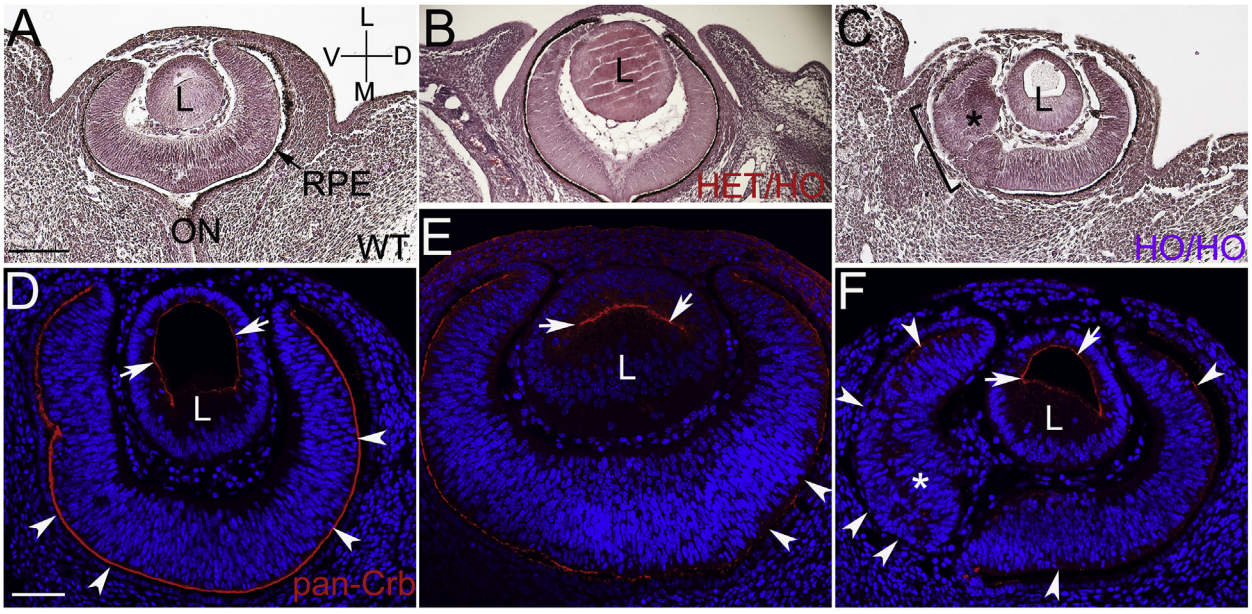

Fig. 8. Crb1/Crb2 dKO (HO/HO) mice show early onset retinal dysplasia and pigmentation defects at E12.5. (A–C) H&E staining of WT (A), HET/HO (B), and HO/HO (B) shows abnormally laminated retina (*) and absent RPE pigmentation (bracket) at E12.5. The orientation of the eye is indicated by V (ventral), D (dorsal), M (medial) and L (lateral). (D & E) α-pan-Crb signal is normal and mildly reduced in the apical surface of the retinal epithelium in WT and HET/HO (arrowheads, D and E), respectively. (F) In HO/HO retinas, α-pan-Crb signal is severely reduced at the junctions of apical borders of retina (arrowheads, F). In the lens vesicle, where Cre is not expressed, α-pan-Crb signal is unaltered in HO/HO retinas compared to WT and HET/HO (arrows, D - F). Abnormal epithelial lamination is evident in HO/HO retinas by Hoechst staining (*). Scale bars, 100 μm (A–C) and 50 μm (D–F). L, lens, ON, optic nerve; RPE, retinal pigment epithelium.

the mature retina (den Hollander et al., 2008; Kumaran et al., 2017). Although development of gene- and cell-based therapies relies heavily on model systems that faithfully replicate and increase understanding of the pathophysiology of the human disease, the available experimental models for LCA8 are inadequate. Mutations in Crumbs genes, Crb1 and Crb2, are responsible for another related degenerative retinal disease, RP12, in addition to LCA8. In the present study, to investigate the function and contribution of individual genes, we modeled RP12 and/or LCA8 by generating a series of multiple bi-allelic mutations of Crb1 and Crb2 that cause differential deletion specifically in developing ocular tissues (neural retina and RPE) beginning at the optic vesicle stage. Our approach induced a significantly earlier onset of blindness and unique retinal lesions in Crb1/Crb2 dKO. We found that the specific phenotypes of Crb1/Crb2 dKO included indistinct retinal lamination with randomly distributed progenitor and photoreceptor cells during and after development, formation of retinal spots enriched with neuronal processes but distinct from retinal rosettes, and temporary thickening of the central retina at P21. The appearance of RPE pigmentation was also altered at E12.5: pigmentation was either absent or severely diminished. Furthermore, the ERG response was nearly absent as early as P14/P15/P16, in the eye opening stage, in Crb1/Crb2 dKO, but not in others of the allelic series (mutants mimicking RP pathology). These findings illustrate a remarkable phenotypic resemblance between Crb1/Crb2 dKO and human LCA8 and suggest that a nearly complete loss of Crb1 and Crb2 is the prerequisite for inducing LCA8 pathology in the mouse.

Our study suggests that the functional compensation of Crb1 deficiency by Crb2 differs in mice compared to humans and the loss of both genes are absolute requirement to induce LCA8 phenotype. In humans, whereas Crb1 mutations cause a spectrum of ocular defects in humans, including RP12 and LCA8, only 10–20% of individuals with Crb2 mutations exhibit milder eye defects, such as reduced visual acuity, abnormal retinal pigmentation, and optic atrophy, in addition to renal disease and ventriculomegaly/hydrocephalus (Chen et al., 2019; Lamont et al., 2016). This is somewhat unexpected considering that, like Crb1, which is expressed most strongly in the human retina and brain, Crb2 is also predominantly expressed in human fetal eye and RPEs, in addition to brain, kidney, heart and lung (Roh et al., 2002; van den Hurk et al., 2005; Watanabe et al., 2004). In the Crb1^{rd8} mouse where Crb1 is deficient, Crb2 is 1.5-fold upregulated in the cortex, which is thought to attribute to the lack of cortical defects in the mutant (Dolon et al., 2018).

It is even more puzzling that three mouse Crb1 mutants, including the null allele, do not show any of the features of human LCA8, and, instead, express the characteristics of RP12: late-onset and relatively mild retinal pathology, including laminar disorganization in ONL manifested by rosettes and half-rosettes (Aleman et al., 2011; van de Pavert et al., 2004). Moreover, 9 -18 month-old Crb1 mutant mice do not show visual impairment (Aleman et al., 2011; Markand et al., 2016). This variance from humans may be attributable to the species difference. For example, the two species may differ in their mode of functional complementation between Crb1 and Crb2. While human Crb2 is not capable of compensating Crb1 loss, it is possible that mouse Crb2 readily substitutes for loss of Crb1 during development. Alternatively, functional conversion between Crb1 and Crb2 may occur during evolution. If so, then human Crb1 would function more like mouse Crb2 and vice versa. Our genetic study would support either explanation. First, our observation that the Crb2 cKO (WT/HO) retinal phenotype is more severe than that of Crb1 (HO/WT), indicates that Crb2 is more crucial than Crb1 in mouse eye development. Second, we found that the Crb2 phenotype can be enhanced by introducing Crb1 heterozygous or homozygous mutations; WT/HO < HET/HO < HO/HO. This result suggests that normal Crb1 can functionally compensate for Crb2 deficiency. The reverse is also true, because the Crb1 phenotype is enhanced when one or two Crb2 mutations are introduced: HO/WT < HO/HET < HO/HO. Because the Crb3 gene encodes Crb1/Crb2 homologs in mouse and human genomes, we cannot completely exclude possible compensation by Crb3 or a complex genetic interaction. However, it is conceivable that Crb3 may not fully compensate the loss of Crb1, 2 or 1/2 because it lacks the large extracellular domain that both Crb1 and Crb2 share and which is essential for cell-cell interaction. Therefore, it is highly plausible that, although human LCA8 is caused by mutations in Crb1 gene, mouse Crb1 mutations, including complete loss of function mutations, are insufficient to induce severe, early-onset LCA8 pathology. Instead, our genetic study

comparing bi-allelic series of Crb1 and Crb2 mutations supports the notion that both Crb1 and Crb2 mutations are necessary to induce LCA8 in the mouse when gene ablation is initiated at the optic vesicle stage.

Similar to the longitudinal study of human patients with RP12 that revealed progressive deterioration of visual acuity and increased retinal thinning with aging (Mathijssen et al., 2017), our study of HET/HO mouse found severe retinal thinning and nearly absent ERG responses in adult stages. For example, HET/HO, but not other bi-allelic combinations except HO/HO, showed markedly reduced scotopic a- and b-wave peak latency and amplitudes, defective optokinetic responses, extensive retinal lesions, and reduction of retinal function (OKR and ERG), all of which were more severe at the adult stage than before. Therefore, HET/HO mice likely represent the severe form of RP. This interpretation is supported by previous observations: Crb1 mutant is likely to represent extremely weak (and rare) mutations of human RP12 because it exhibits limited and mild retina disorganization (Mehalow et al., 2003; Pellissier et al., 2013; van de Pavert et al., 2004, 2007). Crb2 cKO mice show a severe phenotype with progressive loss of photoreceptor cells and visual activity, thus mimicking RP12 (Alves et al., 2013a; Pellissier et al., 2013). Intriguingly, only HO/HO, but not HET/HO, mice, showed similar functional attenuation at P14 – P16, the eye opening stage; and only HO/HO retinas had defective pigmentation at early stages. Therefore, it is highly likely that HET/HO exemplifies the severe cases of RP12, other Crb1/Crb2 mutants (HO/WT, HO/HET, and WT/HO) represent weaker cases of RP12, and that HO/HO represents the severe form of LCA8 with early-onset.

A majority of LCA8 patients have a thicker than normal central retina, which makes them unique among LCA patients; retinas are commonly thinned in other types due to progressive retinal degeneration (Aleman et al., 2011; Jacobson et al., 2003; Kumaran et al., 2017). However, thinning did not correlate with patient age, which normally reflects the degree of retinal degeneration (Aleman et al., 2011). Intriguingly, while all the examined LCA8 patients had hyper-thickness, some showed progressive retinal thinning while others did not show a decrease in retinal thickness. The present study found that only HO/HO (Crb1/Crb2 dKO), but not HET/HO, retinas were thickened at two central locations surrounding the optic disc at P21, but not at P0, which may recapitulate another feature of human LCA8 patients. Retinal thickening was also observed in Crb1/Crb2 cKO (Chx10-Cre), but not in Crb2 cKO, which demonstrated progressive thinning of ONL and OPL (Alves et al., 2013a; Pellissier et al., 2013). Thickening was apparent in Crb1/Crb2 cKO (Chx10-Cre) retinas at P10 and P14, but these retinas gradually became thinner after one month of age (3–6 months). This study did not examine the entire thickness and length of the retina, but, similar to our results, it also showed by OCT that at one month the GCL was disorganized and abnormally thickened, with one plexiform layer and one nuclear layer. HO/HO retinas were thinner than WT in general at adult stages, however, and significantly thinner at three positions, including one central and two peripheral. HET/HO retinas were significantly thinner than those of WT and HO/HO. Thinning observed in HET/HO and HO/HO may indicate progression of retinal degeneration at various adult stages. This interpretation is partly supported by drastic increase of CC3+ cells in HET/HO and HO/HO at adult stage, but not at P21. While it has been proposed that thickened retinas of Crb1/Crb2 cKO (Chx10-Cre) might be due to an increased number of Otx2+ late-born precursor cells (Pellissier et al., 2013), the exact cause of the retinal thickening in LCA8 is not clear. Because the thickness of the plexiform layer was dramatically increased, it is plausible that ectopic growth and/or disorganization of neuronal processes may have made an important contribution.

Another unique morphological feature of the LCA8 retina is the presence of retinal spots. In this study, the retinal spots that we frequently observed in HO/HO were qualitatively different from the rosettes that were common in HET/HO or other RP12 models. Intriguingly, a marker of retinal processes, such as PKCα, was enriched in the spots. In addition, unlike the rosettes commonly observed in Crb1 mutant retinas and in the retinas of other series of Crb1/Crb2 mutants, these spots were not surrounded by photoreceptors, and did not contain OLM, MG endfeet, or OS (absence of signals for Pals1/pan-Crb, GS + endfeet, and Rhodopsin). Instead, they were surrounded by Pax6+ cells. This observation indicates that the spots observed in HO/HO are not rosettes. It will therefore be of great interest in the future to determine whether these structures correspond to the hyperreflective spots found in human LCA8 patients by OCT. Intriguingly, these spots first appeared in neonatal retinas of HO/HO, although we cannot exclude that they start to form during earlier embryonic stages. Therefore, it will be rewarding to investigate the underlying mechanisms of their formation to better understand the origins of the retinal pathology during development.

We also found photoreceptor cells to be dislocated basally in the HO/HO and to be distributed nearly randomly at P0 and P21, consistent with severely disorganized retinal lamination. This result is also consistent with the previous finding that M-phase cells are localized randomly throughout the entire thickness of the retina in Crb1/Crb2 cKO (Chx10) at E17.5 (Pellissier et al., 2013). It is therefore possible that defective interkinetic nuclear migration of retinal progenitors is responsible for ectopic localization of retinal cells in HO/HO mutants.

Genetic studies of RP12 and LCA8 patients did not identify a clear genotype-phenotype correlation for Crb1 mutations (den Hollander et al., 2004). It is plausible that the degree of gene loss may determine phenotypic manifestation. For example, null mutations of Crb1 might induce severe LCA8 while other hypomorphic alleles might induce mild RP12, a proposal for which genetic studies of human Crb1 patients provide suggestive, but not conclusive evidence (den Hollander et al., 2001). However, this proposition was not fully validated because additional factors that influence phenotypes, including other genetic modifiers and environmental causes, also affect the severity of Crb1 mutant phenotype (Bujakowska et al., 2012; den Hollander et al., 2004; Gosens et al., 2008; Henderson et al., 2011; Richard et al., 2006). The present genetic analysis revealed at least three mutant groups among the combinations of Crb1 and Crb2 mutations that displayed quantitative structural and functional differences in the adult retinas. In general, the degree of gene loss correlated with the degree of the phenotypic manifestation. One group of mutants, consisting of those with loss of one copy of Crb1 or Crb2 (HET/WT or WT/HET), two copies of Crb1 (HO/WT) or one copy of Crb1 and Crb2 (HET/HET), did not express any detectable phenotypes. A second group, consisting of those with loss of two copies of Crb2 (WT/HO) or two copies of Crb1 and one copy of Crb2 (HO/HET), expressed an intermediate level of phenotype. A third group, with loss of one Crb1 and two Crb2 genes (HET/HO) or both copies of Crb1 and Crb2 (HO/HO), exhibited the strongest structural and functional deficits. Intriguingly, while HET/HO and HO/HO were functionally indistinguishable at the adult stage, HO/HO displayed unique structural defects reminiscent of thickened retinas with unclear lamination, pigmentary change of the RPE and selective visual impairment at the eye opening stage, which qualifies it as an appropriate model for LCA8. The observation that only HO/HO mice, and not HET/HO, exhibit RPE-associated defects suggests that Crb1 also plays an important role in RPE cell maintenance in rodents. This role in mice contrasts with that in humans, in whom Crb2 mutation alone is sufficient to induce RPE degeneration. Intriguingly, expression of Crb1 has not been established in the RPE, whereas forms of Crb2 mRNA and proteins have been detected in human and mouse RPE (Paniagua et al., 2015; van den Hurk et al., 2005). Therefore, additional expression and genetic analyses using an RPE-specific Cre driver are needed to clarify the cell-autonomous involvement of Crb1 and Crb2 in RPE pathogenesis.

Our study illustrates the crucial LCA8-specific features in Crb1/Crb2 dKO retinas that are comparable to those of human patients. An LCA8-like phenotype has also been proposed in other conditional mutant series where Crb2 was ablated in different retinal cell populations in a $Crb1^{rd8}$ background, including for example, from Muller glia, immature photoreceptor cells or retinal progenitor cells (Quinn et al., 2019). Deleting Crb2 from retinal progenitor cells with Chx10-Cre produced the earlier onset and strongest retinal phenotype in these mice, indicating

that the timing of the gene ablation is a critical factor. Our mutants deleting Crb2 in the optic vesicle (Crb1/Crb2 dKO) share several phenotypes with the mutant series that have been previously reported. These include defective lamination, ERG reduction, and OLM disruption that are features common to both RP12 and LCA8. Other features, such as transient thickening of the retina and ectopic retinal cell positioning, are subsets of the LCA8 phenotype. Importantly, however, these previously reported mutant series did not express other critical features of the LCA8-specific phenotype, including early onset of the ERG impairment at the eye opening stage, pigmentary defect in the RPE, and acellular retinal patches that may correspond to the hyperreflective spots found in the human disease by OCT. In addition, the phenotype was primarily enriched in the retinal periphery, perhaps because Cre lines exhibit a bias that reflects the progression of retinogenesis from the center to the periphery.

Taken together, our results support the hypothesis that complete loss of both Crb1 and Crb2 in the early ocular progenitor cells in the optic vesicle induces an early-onset, severe form of degenerative retinal disorder, LCA8, whereas partial deletions of Crb1 and/or Crb2 induce models of milder, late-onset forms of RP, RP12. This proposition is also supported by the absence of a gene-specific phenotype; Crb1 and/or Crb2 mutants did not display qualitatively different structural abnormalities, and their retinas contained a variable degree of folding and rosettes. This study used Crb1^{rd8} and conditional mutation of Crb2 that induced a frame shift mutation and generated null mutations by deleting exons 7 and 8 in the Crb2 locus. Therefore, further analyses using site-specific mutations will be necessary to determine whether gene- and/or allele-specific mutations of Crb1 and Crb2 in early ocular progenitor cells contribute to retinal pathology.

4. Materials and methods

4.1. Animals: generation and genotyping of Crb1/Crb2 alleles

All animal handling, housing and experimentation were approved by and conducted under the guidelines of the Temple University Animal Welfare Committee.

Generation of Crb1 floxed allele. Three frozen ES cells purchased from EUCOMM (Clone ID: HEPD0659_7_G11) were cultured and injected into C57BL6 blastocysts at the Fox Chase Cancer Center (Temple University) for the production of the chimeras. One founder male with greater than 60% chimerism, when crossed with C57BL6 females, showed inheritance of agouti coat color and floxed Crb1. Genotyping with primers detecting lacZ, neo cassettes, and FRT sites confirmed the presence of the transgene. Subsequently, PCR using designed primers flanking the loxP site (See above) verified this result. Because JM8A3.N1, which is known to contain an rd8 mutation with C57BL6/N background (Mattapallil et al., 2012), was present in the ES cells, the Crb1 flox allele used in this study also has rd8. All mice containing the Crb1 flox allele were positive for the rd8 allele (see genotype section).

Generation of Crb2 floxed allele. Frozen sperm with the Crb2 flox allele was purchased from KOMP (KO-5350-3) and used to fertilize oocytes from C57BL6/N females *in vitro*; two-cell embryos were transferred to C57BL6 females (University of Wisconsin-Madison Research Animal Resource Center). Multiple pups were produced and genotyped for the presence of the lacZ, neo cassettes, and FRT sites as described above.

Resulting mice were crossed to transgenic mice ubiquitously expressing Flpe, flippase recombinase (Flp) (Rodriguez et al., 2000), which recognizes FRT sites, to remove a Neo cassette containing IRES-LacZ, hbactP-Neo flanked by FRT sequences. Resultant mice, which are designated as flox alleles of Crb1 and Crb2, were crossed to a Cre driver for tissue-specific gene ablation. The mRX-Cre line was previously described (Klimova et al., 2013). The presence and absence of mRX-Cre was determined by PCR analysis, using two primers (Klimova et al., 2013) (sense: 5′-AGCACCAAAGCTCCAGTTACC-3’; antisense: 5′-CGTTGCATCGACCGGTAATGCA-3′). PCR genotyping was done using the following primer sets. For Crb1 genotyping; C: 5′-GTATGAGCACAGGCAGCCCT-3’. D: 5′-AGCTGCTGCTTGTGAGGATC-3’. For Crb2 genotyping; E: 5′-GAGTGGCTTGGAGAGAGTCCTT-3’. F: 5′-TGTCTG GGTCAGGATGC-3’. PCR conditions were; 94 °C for 30 s, 60 °C for 1 min, 72 °C for 45 s; total PCR cycle was 40. The presence of rd1 and rd8 alleles, mutations that are frequently observed in generally used WT strains and ES cells commonly used to generate flox alleles, was determined as described (Gimenez and Montoliu, 2001; Kim et al., 2016; Mattapallil et al., 2012).

5. Histology and immunofluorescence (IF)

The entire embryo and enucleated eyes of postnatal mice were fixed with 4% paraformaldehyde in PBS and embedded in paraffin to prepare 6–7 μm sections. Briefly, tissue sections were then deparaffinized and rehydrated by washing in xylene (3X, 5 min), xylene/ethanol (50:50, 5 min), an ethanol series (100%, 95% and 70%, 1X, 3 min), and deionized distilled water (3 min). Rehydrated slides were stained with hematoxylin for 2 min, rinsed in tap water for 3 min, stained with eosin for 1 s, and dehydrated with washes in an ethanol series (95%, 1X, 3 min; 100%, 2X, 3 min), xylene/ethanol (50:50, 2 min), and xylene (2X, 2 min). They were then cleared with Citrus Cleaning Solvent (2X, 2 min, Richard Allan Scientific) and mounted on a coverslip with a drop of Cytoseal (Richard Allan Scientific).

Paraffin sections were subjected to extensive antigen retrieval using citric acid (Park et al., 2016), followed by incubation with a primary antibody overnight at 4 °C. After three washes in phosphate buffered saline, the slides were incubated with a secondary antibody diluted 1:200 in blocking buffer for 2 h at room temperature. Nuclear counterstaining was done with Hoechst 33342 (1:1000, Invitrogen, Carlsbad, CA, USA) before mounting the cover slips with Fluoro-G* slide-mounting medium (Southern Biotech, Inc., Birmingham, AL, USA). Imaging was done using a confocal microscope (TCS SP8, Leica Microsystems GmbH, Wetzler, Germany) and an Axioplan 2 (Carl Zeiss Microimaging GmbH, Germany).

6. Antibodies

Primary antibodies used in this study were: calbindin (mouse, 1:200, Sigma-Aldrich), calretinin (mouse, 1:200, EMDMillipore, USA), CC3 (rabbit, 1:200, Cell Signaling Technology, Danvers, MA, USA), Chx10 (sheep, 1:200, Exalpha, Shirley, MA, USA), cone arrestin (rabbit, 1:200, EMDMillipore), pan-Crb (rabbit, 1:200, synthesized using an epitope located at the C-terminus of mouse Crb1: VGARVPPTPNLKLPPEERLI (Makarova et al., 2003), GFAP (mouse, 1:200, Thermo Fisher Scientific, Fremont, CA USA), GS (mouse, 1:200, BD Biosciences), Iba1 (rabbit, 1:200, Wako Pure Chemical Industries, Ltd, Richmond, VA, USA), Pals1 (rabbit, 1:200, EMDMillipore), Pax6 (rabbit, 1:200, Covance, Emeryville, CA, USA), PKCα (mouse, 1: 200, BD), Rhodopsin (mouse, 1:200, Phosphosolutions, Aurora, CO, USA), pS6 (rabbit, 1:200, CST), Sox9 (rabbit, 1:200, EMDMillipore), and β–III–tubulin (mouse, 1:200, Covance, USA). Secondary antibodies used were Alexa488-conjugated anti-mouse and anti-rabbit antibodies (Life Technologies, USA) and Cy3-conjugated anti-rabbit, anti-mouse and anti-sheep antibodies (Jackson ImmunoResearch Laboratories, Inc., West Grove, PA, USA).

7. Quantification of retinal lesions

From the entire collection of 7 μm paraffin sections from a single eye, we analyzed every 10th slide (14–25 slides per eye) after H&E staining. First, the length of the OLM (the distance from one ora serrata to the other on the opposite side of the section) was determined on each slide using the segmented tracing plugin function of ImageJ. Second, the length of the OLM overlying the retinal area displaying dysplasia was determined similarly from the same slide. For dysplastic areas that were not continuous, but dispersed throughout the retinal sections, the sum of

the dispersed OLM length was used. The mean percent of OLM length associated with retinal dysplasia over total OLM length was used as an index of the retinal lesion for the given eye. Types of retinal dysplasia incorporated in the assay included absence or fusion of ONL and/or INL, diffused/dispersed pattern of retinal cells, rosettes, partial or complete breakdown of OLM shown by apical protrusion of ONL cells, and total absence of OLM.

8. Determination of retinal thickness and detection of apoptotic cells

H&E stained sections were inspected to obtain central retinal sections cut through the center of the eye containing optic disc and a minimum length of ciliary body/iris. The lengths of the OLM between the two retinal tips (ora serrata) and the center of the optic nerve were determined as described. The OLM length of each retinal leaflet was divided by 5.5 to determine the interval between the 5 locations where the thickness was measured (Fig. 4). Due to the variations in retinal thickness at/around the optic nerve, measurement was avoided in this region. The thickness at the tip was measured 25 μm away from the actual tip. Thickness was determined by measuring the vertical distance from OLM to ILM at 12 locations on each section. Mean thickness at 12 locations determined from at least 5 eyes of each genotype was plotted. To detect apoptotic cells showing caspase 3 activation, retinal paraffin sections were stained with α-CC3 following immunofluorescence assay procedures. The numbers of CC3+ cells in the frame were determined and plotted at P21 and adult.

9. Determination of rod cell position; binning and quantification of rod cells

In order to quantitatively evaluate normal and abnormal positioning of rod cells, retinas at P0 were divided into 4 bins. ONBL was equally divided into 3 bins and IPL and GCL were included in bin 4. The number of rod cell bodies (round appearance with bipolar processes) in each bin was counted. At P21, the entire retinal thickness was equally divided into 3 bins. In WT, bin 1 and 2 included ONL and INL, respectively, while bin 3 included the majority of IPL and the entire GCL.

10. Electroretinography

Scotopic and photopic ERGs were performed using the Ganzfeld ERG (Retiport21, Germany). After dark-adaptation for at least 30 min, each mouse was anesthetized with an IP injection of ketamine (80 mg/kg) and xylazine (10 mg/kg), and its pupils dilated with a single drop of topical phenylephrine (2.5%) and tropicamide (mydriacyl) (0.5%). Electrodes were connected to a mouse placed on a stage: two active contact lens-type electrodes were placed on the right and left corneas; two needle-type reference electrodes were placed behind the ears; a needle-type ground electrode was placed near the base of the tail. The time course of the electric current generated by retinal cells after exposure to white light flashes was recorded. The intensity of the light emitted from the Ganzfeld varied from 0.001 cd/m^2 to 10 cd/m^2 (0.001. 0.01, 0.1, 1 and 10) and flashed at a rate of 1Hz, enabling the determination of a-wave and b-wave amplitudes. After light adaptation for 10 min at a background intensity of 25 cd/m^2, photopic ERG was measured. The intensity of the input light was 0.1, 1 and 10 cd s/m^2; the same flash rate setting was used in photopic and scotopic conditions. The responses were averaged from 30 trials at each input light intensity for scotopic and photopic ERGs.

11. Optokinetic response assay

Visual behavior of the Crb1/Crb2 mutant mice was determined by measuring optokinetic responses with OptoMotry (Cerebral Mechanics, Lethbridge, Canada)) following the protocol described elsewhere (Douglas et al., 2005; Ku et al., 2015; Mookherjee et al., 2015; Prusky et al., 2004). Briefly, the mouse was placed on a platform located at the center of the chamber surrounded by four computer screens generating a virtual image of a vertical, black and white grating pattern that drifted at a constant speed around the quad-display configuration. The head tracking of the drifting gratings by the mouse was monitored at a given frequency under photopic conditions through a camcorder placed on top of the chamber and scored by its head movements. Increasing the frequency increases the number of black and white gratings thereby making it more difficult for the mouse to track the moving bars. The threshold spatial frequency, or the maximum frequency at which the mouse could track the pattern, was determined using the random staircase paradigm. Counterclockwise and clockwise rotation elicits independent tracking for the right and left eye respectively. To determine the threshold contrast, the spatial frequency was set to 0.2 cyc/deg. However, the screen contrast varied (following the random staircase paradigm) from 100%, where the screens were unchanged, to 0%, where the screens were completely white.

12. Statistics

Statistical analyses were done on Excel using two-tailed, unpaired t-tests to compare WT and mutants. All data are presented as mean ± standard error from at least three independent analyses (see details in the text). Statistical significance was based on *$p < 0.05$; **$p < 0.01$; ***$p < 0.001$.

Acknowledgements

This work was supported by National Institutes of Health grants R01EY020578 (S.-H.C.) and R01NS104038 (S.K.), by Curing Retinal Blindness Foundation (S.-H.C.), by Shriners Hospitals for Children Research grants 86100 and 85109 (S.K.), and by Czech Ministry of Education, Youth and Sports grant LO1419 (Z.K.).

Appendix A. Supplementary data

Supplementary data to this article can be found online at https://doi.org/10.1016/j.ydbio.2019.05.008.

Conflicts of interest

None declared.

References

Aleman, T.S., Cideciyan, A.V., Aguirre, G.K., Huang, W.C., Mullins, C.L., Roman, A.J., Sumaroka, A., Olivares, M.B., Tsai, F.F., Schwartz, S.B., Vandenberghe, L.H., Limberis, M.P., Stone, E.M., Bell, P., Wilson, J.M., Jacobson, S.G., 2011. Human CRB1-associated retinal degeneration: comparison with the rd8 Crb1-mutant mouse model. Investig. Ophthalmol. Vis. Sci. 52, 6898–6910.

Ali, M.U., Rahman, M.S.U., Cao, J., Yuan, P.X., 2017. Genetic characterization and disease mechanism of retinitis pigmentosa; current scenario. 3 Biotech 7, 251.

Alves, C.H., Bossers, K., Vos, R.M., Essing, A.H., Swagemakers, S., van der Spek, P.J., Verhaagen, J., Wijnholds, J., 2013a. Microarray and morphological analysis of early postnatal CRB2 mutant retinas on a pure C57BL/6J genetic background. PLoS One 8, e82532.

Alves, C.H., Pellissier, L.P., Vos, R.M., Garcia Garrido, M., Sothilingam, V., Seide, C., Beck, S.C., Klooster, J., Furukawa, T., Flannery, J.G., Verhaagen, J., Seeliger, M.W., Wijnholds, J., 2014a. Targeted ablation of Crb2 in photoreceptor cells induces retinitis pigmentosa. Hum. Mol. Genet. 23, 3384–3401.

Alves, C.H., Pellissier, L.P., Wijnholds, J., 2014b. The CRB1 and adherens junction complex proteins in retinal development and maintenance. Prog. Retin. Eye Res. 40, 35–52.

Alves, C.H., Sanz, A.S., Park, B., Pellissier, L.P., Tanimoto, N., Beck, S.C., Huber, G., Murtaza, M., Richard, F., Sridevi Gurubaran, I., Garcia Garrido, M., Levelt, C.N., Rashbass, P., Le Bivic, A., Seeliger, M.W., Wijnholds, J., 2013b. Loss of CRB2 in the mouse retina mimics human retinitis pigmentosa due to mutations in the CRB1 gene. Hum. Mol. Genet. 22, 35–50.

Assemat, E., Bazellieres, E., Pallesi-Pocachard, E., Le Bivic, A., Massey-Harroche, D., 2008. Polarity complex proteins. Biochim. Biophys. Acta 1778, 614–630.

Astuti, G.D., Bertelsen, M., Preising, M.N., Ajmal, M., Lorenz, B., Faradz, S.M., Qamar, R., Collin, R.W., Rosenberg, T., Cremers, F.P., 2016. Comprehensive genotyping reveals

RPE65 as the most frequently mutated gene in Leber congenital amaurosis in Denmark. Eur. J. Hum. Genet. : EJHG 24, 1071–1079.
Bujakowska, K., Audo, I., Mohand-Said, S., Lancelot, M.E., Antonio, A., Germain, A., Leveillard, T., Letexier, M., Saraiva, J.P., Lonjou, C., Carpentier, W., Sahel, J.A., Bhattacharya, S.S., Zeitz, C., 2012. CRB1 mutations in inherited retinal dystrophies. Hum. Mutat. 33, 306–315.
Campanale, J.P., Sun, T.Y., Montell, D.J., 2017. Development and dynamics of cell polarity at a glance. J. Cell Sci. 130, 1201–1207.
Chacon-Camacho, O.F., Zenteno, J.C., 2015. Review and update on the molecular basis of Leber congenital amaurosis. World J. Clin. Cases 3, 112–124.
Chang, B., Hurd, R., Wang, J., Nishina, P., 2013. Survey of common eye diseases in laboratory mouse strains. Investig. Ophthalmol. Vis. Sci. 54, 4974–4981.
Chen, X., Jiang, C., Yang, D., Sun, R., Wang, M., Sun, H., Xu, M., Zhou, L., Chen, M., Xie, P., Yan, B., Liu, Q., Zhao, C., 2019. CRB2 mutation causes autosomal recessive retinitis pigmentosa. Exp. Eye Res. 180, 164–173.
Chen, Y., Zhang, Q., Shen, T., Xiao, X., Li, S., Guan, L., Zhang, J., Zhu, Z., Yin, Y., Wang, P., Guo, X., Wang, J., Zhang, Q., 2013. Comprehensive mutation analysis by whole-exome sequencing in 41 Chinese families with Leber congenital amaurosis. Investig. Ophthalmol. Vis. Sci. 54, 4351–4357.
Coscas, G., De Benedetto, U., Coscas, F., Li Calzi, C.I., Vismara, S., Roudot-Thoraval, F., Bandello, F., Souied, E., 2013. Hyperreflective dots: a new spectral-domain optical coherence tomography entity for follow-up and prognosis in exudative age-related macular degeneration. Ophthalmologica. Journal international d'ophtalmologie. International journal of ophthalmology. Zeitschrift fur Augenheilkunde 229, 32–37.
Coussa, R.G., Lopez Solache, I., Koenekoop, R.K., 2017. Leber congenital amaurosis, from darkness to light: an ode to Irene Maumenee. Ophthalmic Genet. 38, 7–15.
Cremers, F.P., van den Hurk, J.A., den Hollander, A.I., 2002. Molecular genetics of Leber congenital amaurosis. Hum. Mol. Genet. 11, 1169–1176.
den Hollander, A.I., Davis, J., van der Velde-Visser, S.D., Zonneveld, M.N., Pierrottet, C.O., Koenekoop, R.K., Kellner, U., van den Born, L.I., Heckenlively, J.R., Hoyng, C.B., Handford, P.A., Roepman, R., Cremers, F.P., 2004. CRB1 mutation spectrum in inherited retinal dystrophies. Hum. Mutat. 24, 355–369.
den Hollander, A.I., Ghiani, M., de Kok, Y.J., Wijnholds, J., Ballabio, A., Cremers, F.P., Broccoli, V., 2002. Isolation of Crb1, a mouse homologue of Drosophila crumbs, and analysis of its expression pattern in eye and brain. Mech. Dev. 110, 203–207.
den Hollander, A.I., Heckenlively, J.R., van den Born, L.I., de Kok, Y.J., van der Velde-Visser, S.D., Kellner, U., Jurklies, B., van Schooneveld, M.J., Blankenagel, A., Rohrschneider, K., Wissinger, B., Cruysberg, J.R., Deutman, A.F., Brunner, H.G., Apfelstedt-Sylla, E., Hoyng, C.B., Cremers, F.P., 2001. Leber congenital amaurosis and retinitis pigmentosa with Coats-like exudative vasculopathy are associated with mutations in the crumbs homologue 1 (CRB1) gene. Am. J. Hum. Genet. 69, 198–203.
den Hollander, A.I., Roepman, R., Koenekoop, R.K., Cremers, F.P., 2008. Leber congenital amaurosis: genes, proteins and disease mechanisms. Prog. Retin. Eye Res. 27, 391–419.
den Hollander, A.I., ten Brink, J.B., de Kok, Y.J., van Soest, S., van den Born, L.I., van Driel, M.A., van de Pol, D.J., Payne, A.M., Bhattacharya, S.S., Kellner, U., Hoyng, C.B., Westerveld, A., Brunner, H.G., Bleeker-Wagemakers, E.M., Deutman, A.F., Heckenlively, J.R., Cremers, F.P., Bergen, A.A., 1999. Mutations in a human homologue of Drosophila crumbs cause retinitis pigmentosa (RP12). Nat. Genet. 23, 217–221.
Dias, M.F., Joo, K., Kemp, J.A., Fialho, S.L., da Silva Cunha Jr., A., Woo, S.J., Kwon, Y.J., 2018. Molecular genetics and emerging therapies for retinitis pigmentosa: basic research and clinical perspectives. Prog. Retin. Eye Res. 63, 107–131.
Dolon, J.F., Paniagua, A.E., Valle, V., Segurado, A., Arevalo, R., Velasco, A., Lillo, C., 2018. Expression and localization of the polarity protein CRB2 in adult mouse brain: a comparison with the CRB1(rd8) mutant mouse model. Sci. Rep. 8, 11652.
Douglas, R.M., Alam, N.M., Silver, B.D., McGill, T.J., Tschetter, W.W., Prusky, G.T., 2005. Independent visual threshold measurements in the two eyes of freely moving rats and mice using a virtual-reality optokinetic system. Vis. Neurosci. 22, 677–684.
Ehrenberg, M., Pierce, E.A., Cox, G.F., Fulton, A.B., 2013. CRB1: one gene, many phenotypes. Semin. Ophthalmol. 28, 397–405.
Farrar, G.J., Carrigan, M., Dockery, A., Millington-Ward, S., Palfi, A., Chadderton, N., Humphries, M., Kiang, A.S., Kenna, P.F., Humphries, P., 2017. Toward an elucidation of the molecular genetics of inherited retinal degenerations. Hum. Mol. Genet. 26, R2–R11.
Foxman, S.G., Heckenlively, J.R., Bateman, J.B., Wirtschafter, J.D., 1985. Classification of congenital and early onset retinitis pigmentosa. Arch. Ophthalmol. 103, 1502–1506.
Gimenez, E., Montoliu, L., 2001. A simple polymerase chain reaction assay for genotyping the retinal degeneration mutation (Pdeb(rd1)) in FVB/N-derived transgenic mice. Lab. Anim. 35, 153–156.
Gosens, I., den Hollander, A.I., Cremers, F.P., Roepman, R., 2008. Composition and function of the Crumbs protein complex in the mammalian retina. Exp. Eye Res. 86, 713–726.
Hamasaki, D.I., Liu, M., Qiu, H., Fujiwara, E., Lam, B.L., 2002. The a-wave latency in control subjects and patients with retinal diseases. Jpn. J. Ophthalmol. 46, 433–442.
Henderson, R.H., Mackay, D.S., Li, Z., Moradi, P., Sergouniotis, P., Russell-Eggitt, I., Thompson, D.A., Robson, A.G., Holder, G.E., Webster, A.R., Moore, A.T., 2011. Phenotypic variability in patients with retinal dystrophies due to mutations in CRB1. Br. J. Ophthalmol. 95, 811–817.
Hurd, T.W., Gao, L., Roh, M.H., Macara, I.G., Margolis, B., 2003. Direct interaction of two polarity complexes implicated in epithelial tight junction assembly. Nat. Cell Biol. 5, 137–142.
Jacobson, S.G., Cideciyan, A.V., Aleman, T.S., Pianta, M.J., Sumaroka, A., Schwartz, S.B., Smilko, E.E., Milam, A.H., Sheffield, V.C., Stone, E.M., 2003. Crumbs homolog 1 (CRB1) mutations result in a thick human retina with abnormal lamination. Hum. Mol. Genet. 12, 1073–1078.
Khan, K.N., Robson, A., Mahroo, O.A.R., Arno, G., Inglehearn, C.F., Armengol, M., Waseem, N., Holder, G.E., Carss, K.J., Raymond, L.F., Webster, A.R., Moore, A.T., McKibbin, M., van Genderen, M.M., Poulter, J.A., Michaelides, M., Consortium, U.K.I.R.D., 2018. A clinical and molecular characterisation of CRB1-associated maculopathy. Eur. J. Hum. Genet. : EJHG 26, 687–694.
Kim, J.Y., Park, R., Lee, J.H., Shin, J., Nickas, J., Kim, S., Cho, S.H., 2016. Yap is essential for retinal progenitor cell cycle progression and RPE cell fate acquisition in the developing mouse eye. Dev. Biol. 419, 336–347.
Klimova, L., Lachova, J., Machon, O., Sedlacek, R., Kozmik, Z., 2013. Generation of mRx-Cre transgenic mouse line for efficient conditional gene deletion in early retinal progenitors. PLoS One 8, e63029.
Kolesnikov, A.V., Fan, J., Crouch, R.K., Kefalov, V.J., 2010. Age-related deterioration of rod vision in mice. J. Neurosci. : Off. J. Soc. Neurosci. 30, 11222–11231.
Ku, C.A., Chiodo, V.A., Boye, S.L., Hayes, A., Goldberg, A.F., Hauswirth, W.W., Ramamurthy, V., 2015. Viral-mediated vision rescue of a novel AIPL1 cone-rod dystrophy model. Hum. Mol. Genet. 24, 670–684.
Kumaran, N., Moore, A.T., Weleber, R.G., Michaelides, M., 2017. Leber congenital amaurosis/early-onset severe retinal dystrophy: clinical features, molecular genetics and therapeutic interventions. Br. J. Ophthalmol. 101, 1147–1154.
Lamont, R.E., Tan, W.H., Innes, A.M., Parboosingh, J.S., Schneidman-Duhovny, D., Rajkovic, A., Pappas, J., Altschwager, P., DeWard, S., Fulton, A., Gray, K.J., Krall, M., Mehta, L., Rodan, L.H., Saller Jr., D.N., Steele, D., Stein, D., Yatsenko, S.A., Bernier, F.P., Slavotinek, A.M., 2016. Expansion of phenotype and genotypic data in CRB2-related syndrome. Eur. J. Hum. Genet. : EJHG 24, 1436–1444.
Letizia, A., Ricardo, S., Moussian, B., Martin, N., Llimargas, M., 2013. A functional role of the extracellular domain of Crumbs in cell architecture and apicobasal polarity. J. Cell Sci. 126, 2157–2163.
Lotery, A.J., Jacobson, S.G., Fishman, G.A., Weleber, R.G., Fulton, A.B., Namperumalsamy, P., Heon, E., Levin, A.V., Grover, S., Rosenow, J.R., Kopp, K.K., Sheffield, V.C., Stone, E.M., 2001. Mutations in the CRB1 gene cause Leber congenital amaurosis. Arch. Ophthalmol. 119, 415–420.
Makarova, O., Roh, M.H., Liu, C.J., Laurinec, S., Margolis, B., 2003. Mammalian Crumbs3 is a small transmembrane protein linked to protein associated with Lin-7 (Pals1). Gene 302, 21–29.
Markand, S., Saul, A., Tawfik, A., Cui, X., Rozen, R., Smith, S.B., 2016. Mthfr as a modifier of the retinal phenotype of Crb1(rd8/rd8) mice. Exp. Eye Res. 145, 164–172.
Mathijssen, I.B., Florijn, R.J., van den Born, L.I., Zekveld-Vroon, R.C., Ten Brink, J.B., Plomp, A.S., Baas, F., Meijers-Heijboer, H., Bergen, A.A., van Schooneveld, M.J., 2017. Long-TERM FOLLOW-UP OF patients with retinitis pigmentosa type 12 caused BY CRB1 mutations: a severe phenotype with considerable interindividual variability. Retina 37, 161–172.
Mattapallil, M.J., Wawrousek, E.F., Chan, C.C., Zhao, H., Roychoudhury, J., Ferguson, T.A., Caspi, R.R., 2012. The Rd8 mutation of the Crb1 gene is present in vendor lines of C57BL/6N mice and embryonic stem cells, and confounds ocular induced mutant phenotypes. Investig. Ophthalmol. Vis. Sci. 53, 2921–2927.
Mehalow, A.K., Kameya, S., Smith, R.S., Hawes, N.L., Denegre, J.M., Young, J.A., Bechtold, L., Haider, N.B., Tepass, U., Heckenlively, J.R., Chang, B., Naggert, J.K., Nishina, P.M., 2003. CRB1 is essential for external limiting membrane integrity and photoreceptor morphogenesis in the mammalian retina. Hum. Mol. Genet. 12, 2179–2189.
Meuleman, J., van de Pavert, S.A., Wijnholds, J., 2004. Crumbs homologue 1 in polarity and blindness. Biochem. Soc. Trans. 32, 828–830.
Mookherjee, S., Hiriyanna, S., Kaneshiro, K., Li, L., Li, Y., Li, W., Qian, H., Li, T., Khanna, H., Colosi, P., Swaroop, A., Wu, Z., 2015. Long-term rescue of cone photoreceptor degeneration in retinitis pigmentosa 2 (RP2)-knockout mice by gene replacement therapy. Hum. Mol. Genet. 24, 6446–6458.
Motta, F.L., Salles, M.V., Costa, K.A., Filippelli-Silva, R., Martin, R.P., Sallum, J.M.F., 2017. The correlation between CRB1 variants and the clinical severity of Brazilian patients with different inherited retinal dystrophy phenotypes. Sci. Rep. 7, 8654.
Paniagua, A.E., Herranz-Martin, S., Jimeno, D., Jimeno, A.M., Lopez-Benito, S., Carlos Arevalo, J., Velasco, A., Aijon, J., Lillo, C., 2015. CRB2 completes a fully expressed Crumbs complex in the Retinal Pigment Epithelium. Sci. Rep. 5, 14504.
Park, R., Moon, U.Y., Park, J.Y., Hughes, L.J., Johnson, R.L., Cho, S.H., Kim, S., 2016. Yap is required for ependymal integrity and is suppressed in LPA-induced hydrocephalus. Nat. Commun. 7, 10329.
Pellissier, L.P., Alves, C.H., Quinn, P.M., Vos, R.M., Tanimoto, N., Lundvig, D.M., Dudok, J.J., Hooibrink, B., Richard, F., Beck, S.C., Huber, G., Sothilingam, V., Garcia Garrido, M., Le Bivic, A., Seeliger, M.W., Wijnholds, J., 2013. Targeted ablation of CRB1 and CRB2 in retinal progenitor cells mimics Leber congenital amaurosis. PLoS Genet. 9, e1003976.
Pellissier, L.P., Lundvig, D.M., Tanimoto, N., Klooster, J., Vos, R.M., Richard, F., Sothilingam, V., Garcia Garrido, M., Le Bivic, A., Seeliger, M.W., Wijnholds, J., 2014. CRB2 acts as a modifying factor of CRB1-related retinal dystrophies in mice. Hum. Mol. Genet. 23, 3759–3771.
Prusky, G.T., Alam, N.M., Beekman, S., Douglas, R.M., 2004. Rapid quantification of adult and developing mouse spatial vision using a virtual optomotor system. Investig. Ophthalmol. Vis. Sci. 45, 4611–4616.
Qiu, H., Fujiwara, E., Liu, M., Lam, B.L., Hamasaki, D.I., 2002. Evidence that a-wave latency of the electroretinogram is determined solely by photoreceptors. Jpn. J. Ophthalmol. 46, 426–432.
Quinn, P.M., Mulder, A.A., Henrique Alves, C., Desrosiers, M., de Vries, S.I., Klooster, J., Dalkara, D., Koster, A.J., Jost, C.R., Wijnholds, J., 2019. Loss of CRB2 in Muller glial cells modifies a CRB1-associated retinitis pigmentosa phenotype into a Leber congenital amaurosis phenotype. Hum. Mol. Genet. 28, 105–123.
Quinn, P.M., Pellissier, L.P., Wijnholds, J., 2017. The CRB1 complex: following the trail of crumbs to a feasible gene therapy strategy. Front. Neurosci. 11, 175.

Richard, M., Roepman, R., Aartsen, W.M., van Rossum, A.G., den Hollander, A.I., Knust, E., Wijnholds, J., Cremers, F.P., 2006. Towards understanding CRUMBS function in retinal dystrophies. Hum. Mol. Genet. 15 (2), R235–R243.

Rodriguez, C.I., Buchholz, F., Galloway, J., Sequerra, R., Kasper, J., Ayala, R., Stewart, A.F., Dymecki, S.M., 2000. High-efficiency deleter mice show that FLPe is an alternative to Cre-loxP. Nat. Genet. 25, 139–140.

Roh, M.H., Makarova, O., Liu, C.J., Shin, K., Lee, S., Laurinec, S., Goyal, M., Wiggins, R., Margolis, B., 2002. The Maguk protein, Pals1, functions as an adapter, linking mammalian homologues of Crumbs and Discs Lost. J. Cell Biol. 157, 161–172.

Rowan, S., Cepko, C.L., 2004. Genetic analysis of the homeodomain transcription factor Chx10 in the retina using a novel multifunctional BAC transgenic mouse reporter. Dev. Biol. 271, 388–402.

Shintani, K., Shechtman, D.L., Gurwood, A.S., 2009. Review and update: current treatment trends for patients with retinitis pigmentosa. Optometry 80, 384–401.

Solovei, I., Kreysing, M., Lanctot, C., Kosem, S., Peichl, L., Cremer, T., Guck, J., Joffe, B., 2009. Nuclear architecture of rod photoreceptor cells adapts to vision in mammalian evolution. Cell 137, 356–368.

Stone, E.M., 2007. Leber congenital amaurosis - a model for efficient genetic testing of heterogeneous disorders: LXIV Edward Jackson Memorial Lecture. Am. J. Ophthalmol. 144, 791–811.

Talib, M., van Schooneveld, M.J., van Genderen, M.M., Wijnholds, J., Florijn, R.J., Ten Brink, J.B., Schalij-Delfos, N.E., Dagnelie, G., Cremers, F.P.M., Wolterbeek, R., Fiocco, M., Thiadens, A.A., Hoyng, C.B., Klaver, C.C., Bergen, A.A., Boon, C.J.F., 2017. Genotypic and phenotypic characteristics of CRB1-associated retinal dystrophies: a long-term follow-up study. Ophthalmology 124, 884–895.

Tepass, U., 2012. The apical polarity protein network in Drosophila epithelial cells: regulation of polarity, junctions, morphogenesis, cell growth, and survival. Annu. Rev. Cell Dev. Biol. 28, 655–685.

Thompson, B.J., Pichaud, F., Roper, K., 2013. Sticking together the Crumbs - an unexpected function for an old friend. Nat. Rev. Mol. Cell Biol. 14, 307–314.

Turgut, B., Yildirim, H., 2015. The causes of hyperreflective dots in optical coherence tomography excluding diabetic macular edema and retinal venous occlusion section sign. Open Ophthalmol. J. 9, 36–40.

van de Pavert, S.A., Kantardzhieva, A., Malysheva, A., Meuleman, J., Versteeg, I., Levelt, C., Klooster, J., Geiger, S., Seeliger, M.W., Rashbass, P., Le Bivic, A., Wijnholds, J., 2004. Crumbs homologue 1 is required for maintenance of photoreceptor cell polarization and adhesion during light exposure. J. Cell Sci. 117, 4169–4177.

van de Pavert, S.A., Meuleman, J., Malysheva, A., Aartsen, W.M., Versteeg, I., Tonagel, F., Kamphuis, W., McCabe, C.J., Seeliger, M.W., Wijnholds, J., 2007. A single amino acid substitution (Cys249Trp) in Crb1 causes retinal degeneration and deregulates expression of pituitary tumor transforming gene Pttg1. J. Neurosci. : Off. J. Soc. Neurosci. 27, 564–573.

van den Hurk, J.A., Rashbass, P., Roepman, R., Davis, J., Voesenek, K.E., Arends, M.L., Zonneveld, M.N., van Roekel, M.H., Cameron, K., Rohrschneider, K., Heckenlively, J.R., Koenekoop, R.K., Hoyng, C.B., Cremers, F.P., den Hollander, A.I., 2005. Characterization of the Crumbs homolog 2 (CRB2) gene and analysis of its role in retinitis pigmentosa and Leber congenital amaurosis. Mol. Vis. 11, 263–273.

van Rossum, A.G., Aartsen, W.M., Meuleman, J., Klooster, J., Malysheva, A., Versteeg, I., Arsanto, J.P., Le Bivic, A., Wijnholds, J., 2006. Pals1/Mpp5 is required for correct localization of Crb1 at the subapical region in polarized Muller glia cells. Hum. Mol. Genet. 15, 2659–2672.

Verbakel, S.K., van Huet, R.A.C., Boon, C.J.F., den Hollander, A.I., Collin, R.W.J., Klaver, C.C.W., Hoyng, C.B., Roepman, R., Klevering, B.J., 2018. Non-syndromic retinitis pigmentosa. Prog. Retin. Eye Res. 66, 157–186.

Wang, Q., Margolis, B., 2007. Apical junctional complexes and cell polarity. Kidney Int. 72, 1448–1458.

Watanabe, T., Miyatani, S., Katoh, I., Kobayashi, S., Ikawa, Y., 2004. Expression of a novel secretory form (Crb1s) of mouse Crumbs homologue Crb1 in skin development. Biochem. Biophys. Res. Commun. 313, 263–270.

Zulliger, R., Lecaude, S., Eigeldinger-Berthou, S., Wolf-Schnurrbusch, U.E., Enzmann, V., 2011. Caspase-3-independent photoreceptor degeneration by N-methyl-N-nitrosourea (MNU) induces morphological and functional changes in the mouse retina. Graefe's archive for clinical and experimental ophthalmology = Albrecht von Graefes Archiv fur klinische und experimentelle Ophthalmologie 249, 859–869.